AIMS Microbiology

AIMS Microbiology, 12(4): 902–933.
DOI: 10.3934/microbiol.2026038
Received: 06 May 2026
Revised: 21 September 2026
Accepted: 27 October 2026
Published: 10 November 2026

https://www.aimspress.com/journal/microbiology

Research article

Wound-healing, antibacterial, and immunomodulatory effects of *Laevicaulis alte* slug extract: An Integrated *in vitro*, *in vivo*, and *in silico* study

Mostafa Yahia Morad[1,*], Heba El-Sayed[2,*], Ahmed A. Elhenawy[3,4], Hana Sonbol[5], Olfat Hammam[6], Asmaa F. Abdelmonem[2], Amina Ibrahim[7] and Marwa A. Hamada[2,*]

[1] Zoology and Entomology Department, Faculty of Science, Capital University (Formerly Helwan University), Helwan 11795, Egypt
[2] Botany and Microbiology Department, Faculty of Science, Capital University (Formerly Helwan University), Helwan 11795, Egypt
[3] Chemistry Department, Faculty of Science, Al-Azhar University, Nasr City, Cairo 11884, Egypt
[4] Chemistry Department, Faculty of Science and Art, Al Baha University, P.O. Box 1988, Mukhwah, Al Baha 6531, Saudi Arabia
[5] Department of Biology, College of Science, Princess Nourah bint Abdulrahman University, P.O. Box 84428, Riyadh 11671, Saudi Arabia
[6] Pathology Departments, Theodor Bilharz Research Institute, Giza 12411, Egypt
[7] Medical Malacology Department, Theodor Bilharz Research Institute, Giza 12411, Egypt

* **Correspondence:** Email: HebaElSayed@science.capu.edu.eg; mustafa_ali@science.capu.edu.eg; marwa.hamada@science.capu.edu.eg.

Abstract: Wound infections, particularly those caused by bacteria such as *Staphylococcus aureus*, present a significant challenge to effective healing, often leading to chronic inflammation and tissue damage. Finding naturally active new substances and applying them as wound healing agents to decrease bacterial infection and accelerate wound healing is among the most significant areas of research. This study explored the therapeutic potential of a chloroform extract from the terrestrial slug *Laevicaulis alte* as a multifunctional agent for wound care. The investigation integrated chemical profiling by gas chromatography-mass spectrometry (GC-MS), *in vitro* antibacterial evaluation, an *in vivo* excisional wound healing model, and *in silico* molecular docking to elucidate its mechanisms of action. Thirty healthy male Swiss albino mice were randomly allocated to three groups (n = 10/group):

Negative control, positive control treated with gentamicin, and *L. alte*-extract-treated animals. The extract-treated group received 20 μL of *L. alte* extract (625 μg/mL) topically, once daily, for 14 days. GC–MS analysis identified 12 compounds, with tris(2,4-di-tert-butylphenyl) phosphate (TDTBPP) and cholesterol being the most abundant detected constituents. The extract exhibited antibacterial activity against *S. aureus* ATCC 6538, with a minimum inhibitory concentration (MIC) of 0.625 mg/mL. In the infected wound model, topical treatment was associated with accelerated wound closure, reaching 84.4% after 14 days compared with 41.1% in the negative-control group, together with a reduction in wound bacterial burden. Treatment was also associated with reduced levels of the pro-inflammatory cytokines IL-6 and TNF-α and increased IL-10 levels compared with the negative control. Molecular docking predicted favorable interactions between several identified compounds and bacterial DNA gyrase and selected cytokine targets; however, these computational findings require experimental validation. Overall, the findings support the potential of *L. alte* extract as a candidate source of antibacterial and wound-healing activity, while further studies are required to establish the contribution and mechanisms of individual constituents.

Keywords: slugs; *Laevicaulis alte*; *Staphylococcus aureus*; wound healing; antibacterial; GC-MS; *in silico*

1. Introduction

The skin serves as a primary defense of the immune system. It can defend against bacterial and fungal invasion and perform defensive and protective roles [1]. Skin serves several purposes: It synthesizes vitamin D, maintains body temperature, improves metabolic processes, shields against various types of trauma, including thermal, chemical, and UV radiation, and keeps us in touch with our surroundings through a variety of nerve terminals [2].

Skin wounds are common and a serious public health concern due to their harmful effects on a patients' quality of life. Skin wounds do, in fact, hurt and impair function and mobility, and they can also have an adverse effect on mental health by creating social isolation, melancholy, anxiety, and embarrassment [3]. The skin may be infected with many pathogens such as viruses, bacteria, fungi, and parasites. Bacterial skin infections are frequently observed in tropical areas due to the humidity and ambient temperature, which can sometimes be associated with poor hygiene. Moreover, the rich supply of nutrients, water, and high temperature found in the skin makes it a perfect medium for microbial growth [4].

A wide range of cellular activities support the complex, dynamic process of wound healing, which requires careful coordination to properly repair damaged tissue [5]. To complete the healing process, the skin passes through four stages: Homeostatic, inflammatory, proliferative, and remodeling [4]. There are two main types of cutaneous wounds based on the degree of pathogenicity and consequences: Acute and chronic. The immune response plays an extremely important role during the phase of wound healing by initiating the inflammatory process, assisting in wound cleaning, and promoting subsequent tissue healing. Conversely, in the course of wound healing, immune system dysregulation during the healing process can result in persistent inflammation and slowed healing, both of which can contribute to chronic wounds [6].

The second-largest phylum in the animal kingdom is called Mollusca. Gastropoda is the largest class and includes 80% of species, which may be snails or slugs, within the phylum Mollusca. Throughout the Nile Delta region and the North Coast belt of the Mediterranean Sea, large numbers of terrestrial gastropod species are economically significant as pests in horticulture and agriculture [7]. Several species of slugs are considered pests in many agricultural fields, causing huge loss in the environmental ecosystem in different parts of the world. Crops, such as soybeans and corn, are damaged by slugs due to their feeding behavior, and the harvested plants can be contaminated with their bodies, eggs, slime, or feces, leading to deterioration in the quality of the harvest and economic loss [8]. Furthermore, the slugs have the potential to restrict the plant's range of dispersion [9] and, by means of selective feeding, modify the composition and abundance of specific plant species [10].

Finding biologically active compounds originating from living animals and using them in biotechnological processes for the food, cosmetic, pharmaceutical, and other industries is one of the most important topics in global research. However, numerous scientific studies have demonstrated snail and slug mucus's cytotoxicity impact on a range of cell lines, but their body extract role in many applications hasn't been elucidated. Organisms that thrive as agricultural pests often possess robust chemical defense mechanisms that enable their survival in challenging, microbe-rich environments [11,12]. Mollusks, including slugs, have evolved complex bioactive secretions for predator deterrence, pathogen resistance, and tissue repair following injury—functions that are directly relevant to wound healing applications [13]. Research has demonstrated that mollusk-derived compounds contain growth factors, extracellular matrix components, and antimicrobial peptides that promote cell proliferation, migration, and tissue regeneration [13,14]. Rather than solely viewing slugs as pests, we recognize them as underexplored sources of bioactive compounds that could be repurposed for therapeutic benefits. This concept of "bioprospecting from invasive species" is a well-established paradigm in natural product research, where organisms typically considered problematic are re-evaluated as valuable bioresources for pharmaceutical, cosmetic, and nutraceutical applications [15].

Therefore, this study aimed to evaluate the slug extract's effective role in promoting wound healing as well as its antimicrobial efficacy against *Staphylococcus aureus* through computational, *in vivo*, and *in vitro* assessments.

2. Materials and methods

2.1. Slug source and extract preparation

Laevicaulis alte slugs (9–10 mm) were reared in the invertebrate lab, Faculty of Science, Capital University (Formerly Helwan University), Egypt. It was kept in 15 × 24 × 10 cm plastic boxes with oven-dried lettuce leaves and de-chlorinated tap water. Slugs were cleaned using distilled water and 70% ethyl alcohol. After complete drying, they were roasted at 37 ℃ for 3 days in an oven; later, they were ground with a 400 mm disc mill (EarthTechnica Co. LTD, Japan). The powdered slugs were submerged in a chloroform solvent (Sigma-Aldrich, United States) (1:2) for two days. Subsequently, the slug particles were removed by centrifugation (Sigma, Germany) at 4472 × g for 10 min at 4 ℃. Then, the chloroform was evaporated using a rotary evaporator (IKA, Germany) and the resulting extract was collected for further assays.

2.2. Slug extract analysis using GC-MS

After the slug extract was prepared, it was dissolved in chloroform to be analyzed using a gas chromatography-mass spectrometry (GC-MS) instrument (Agilent Technologies, Santa Clara, California) at Central Laboratories Network, National Research Centre, Cairo, Egypt. The gas chromatography system was fitted with a 30-meter-long DB-5MS column that had an internal diameter of 0.25 mm and a film thickness of 0.25 μm. The used carrier gas was helium at a flow rate of 2.0 mL/min with a splitless injection volume of 1 μL. The following program of temperature was 50 ℃ for 5 min, rising at 5 ℃/min to 100 ℃ and held for 0 min, and rising at 10 ℃/min to 320 ℃ and held for 10 min. Both the detector and injector temperatures were maintained at 320 ℃ and 280 ℃, respectively. Mass spectra were generated using electron ionization (EI) at 70 eV, covering a spectral range of m/z 25–800 with a solvent delay of 3 min. The mass temperature was set at 230 ℃, and Quad was set to 150 ℃. The identification of various constituents was accomplished by comparing the spectrum fragmentation pattern with those stored in Wiley and NIST Mass Spectral Library data. A GC-MS analysis was performed in triplicate on a single pooled extract, and the reported compositions are mean values. All extraction and processing steps were strictly carried out using pre-cleaned borosilicate glassware to ensure the analytical quality of the chemical profile and to rule out possible laboratory artefacts or plasticizer contamination. Throughout the extraction procedure, commercial synthetic or plastic consumables, tubes, and pipettes were entirely avoided. Additionally, a parallel chloroform blank control was fed into the GC-MS apparatus immediately prior to the sample analysis. No corresponding peak attributable to tris(2,4-di-tert-butylphenyl) phosphate (TDTBPP) was detected in the solvent blank chromatogram. These analytical controls reduced the likelihood of contamination originating from the extraction solvent, analytical system, or plastic consumables.

2.3. Antibacterial activity of slug extract against Staphylococcus aureus

2.3.1. Broth microdilution assay and MIC determination

The examination was carried out employing the broth microdilution method, which was slightly modified from the original protocol [16,17]. To make a stock extract, 2.5 mg of the dried extract was reconstituted in 1 mL of sterile water. The initial column well of a microtiter plate was filled with 400 μL of the obtained stock extract, and each well between 2 and 10 received 200 μL of sterile tryptic soy broth (TSB). By moving 200 μL gently from the first well to the sixth, a twofold dilution was created. Subsequently, 50 μL of the reference strain *S. aureus* ATCC 6538 with a concentration of 5×10^8 CFU/mL (OD~0.1) was applied to each well in a single row, excluding the final well designated as a blank for background correction. Both chloramphenicol (1 mg/mL) and ciprofloxacin (1 mg/mL) were used as a positive control. Following 24 h of incubation at 37 ℃, bacterial growth was assessed by measuring the optical density (OD) at 630 nm using a ChroMate 4300 ELISA reader. The untreated bacterial culture served as the growth control (seventh well). The percentage of bacterial growth/viability was calculated relative to the untreated growth control after correction for background absorbance using the following equation: % viability = $[(OD_{test} - OD_{blank})/(OD_{untreated\ control} - OD_{blank})] \times 100$ [18]. The minimum inhibitory concentration (MIC) assay was performed in three independent experiments, each consisting of three technical replicates (n = 3).

2.4. Wound healing and antibacterial efficacy of slug extract against S. aureus in vivo

2.4.1. Animal ethics committee for mouse models of wound infection

The care and utilization of research animals at Capital Institution followed guidelines that were authorized by the committee of the university's Animal Ethics. All experimental protocols were approved by the Institutional Animal Care and Use Committee (IACUC) of the Faculty of Science, Capital University, with the research study assigned a specific research ethics number [HU-IACUC/Z/MY3107-31]. This study was done in accordance with the ARRIVE guidelines (https://arriveguidelines.org).

2.4.2. Animals

About six-week-old male Swiss albino mice (weighing around 30 ± 2 g) were purchased from the Theodor Bilharez Institute's animal house in Egypt and were acclimatized at the animal house, Zoology and Entomology Department, Faculty of Science, Capital University, for two weeks. The mice stayed in polypropylene cages (ten animals per cage) under typical laboratory conditions: A 12-hour light/dark cycle, a temperature range of 22–25 ℃, and a relative humidity of 50–60%. The animals were provided unrestricted access to regular rodent food (Purina, 20% protein) and tap water ad libitum. All animals were in good health and exhibited no visible signs of infection at the beginning of the study.

2.4.3. Developing excision wound

The full-thickness excisional skin wounds were created on anesthetized mice (using isoflurane), whose dorsal fur was subsequently washed, shaved, and disinfected in preparation for the experiment. An aseptic puncher was employed to produce an oval, full-thickness wound (3 mm) on the upper back of the mice. *Staphylococcus aureus* ATCC 6538 was prepared at a concentration of 5×10^8 CFU/mL, and 20 μL of the bacterial suspension, corresponding to 1×10^7 CFU per wound, was applied to each freshly created wound. The wounds were inoculated 3 hours after wound creation and topical treatment was initiated 24 hours after bacterial inoculation. At the end of the study, all euthanized mice were treated humanely and killed with cervical dislocation to allow for tissue and organ examination, prevent their reintroduction into other experiments, and eliminate potential biohazards if released.

2.4.4. Treatment groups

All experiments were done at the animal house, Zoology and Entomology Department, Faculty of Science, Capital University. Thirty healthy male Swiss albino mice were randomly divided into three experimental groups (n = 10 mice in each group) by a computer-generated random number sequence and housed in different cages, with free-flowing water and unlimited food. The sample size ($n = 10$) was based on prior data and standard protocols from similar peer-reviewed *in vivo* wound healing studies to provide sufficient statistical power while minimizing animal use consistent with ethical standards. There were no pre-determined exclusion criteria and no animals were excluded from the study since all subjects remained healthy and successfully reached the experimental endpoints.

Group I (negative control) included mice with excisional skin wounds treated with phosphate-buffered saline (PBS), group II (positive control) included mice with excisional skin wounds that received gentamicin cream (0.1%), and group III (treated) included mice with excisional skin wounds that received 20 µL slug extract. The slug extract concentration used for topical treatment (625 µg/mL) was selected based on the minimum inhibitory concentration (MIC) determined in the *in vitro* assay against *S. aureus* ATCC 6538 (0.625 mg/mL, equivalent to 625 µg/mL). A volume of 20 µL of the extract was applied topically to each wound once daily for 14 days. This volume contained 12.5 µg of extract per application. Based on the original 3-mm diameter wound (area ≈ 0.0707 cm^2), the applied dose was approximately 176.8 µg/cm^2 of wound surface area per application. The selected topical volume was within the range used in our previous *in vivo* wound-healing study [19]. Treatment administration and daily measurement of wound size were performed by independent investigators to avoid bias, and a histological evaluation was performed by a pathologist blinded to the experimental group allocations.

For histological comparison, a previously prepared and archived section of normal mouse skin tissue maintained in our laboratory was used as a normal histological reference representing the typical architecture of non-wounded mouse skin. The tissue originated from mice with characteristics consistent with those used in the present experiment, namely male Swiss albino mice of approximately six weeks of age and weighing approximately 30 ± 2 g. No additional animals were sacrificed specifically to obtain normal skin tissue for the present study.

The archived normal/reference tissue was solely used to facilitate a qualitative comparison of the histological architecture of the experimental wound tissues. It was not considered an additional experimental group or an independent biological replicate and was therefore not included as a separate group in the statistical analysis. Moreover, the use of archived tissue minimized the need for additional experimental animals and was consistent with the 3Rs principle of Reduction.

2.4.5. Macroscopic estimation of wound size

Following topical application, daily photos of the wound were captured. The wound area was assessed by measuring the distance along the wound bed and delineating a circle around its perimeter [20]. To ascertain each image's magnification during the measurement analysis, a fine ruler was positioned at the wound level to determine its size. The wound healing percentage was calculated according to the following formula 1:

$$\text{Healing Percentage (\%)} = [1 - (\text{wound area})/(\text{original wound area})] \times 100 \text{ [21].} \quad (1)$$

2.4.6. Bacterial load estimation

The following protocol was used for bacterial load determination in both treated (II and III) and untreated (I) groups, according to El-Sayed et al. [19]. The experiment was carried out on both the zero and seventh days of the *in vivo* experiment. After inoculating the wound of the experimental mice with bacteria, disposable medical scalpels were used to excise a 1 mm thick wound from each of the three groups. Then, the samples were put into sterile 1× phosphate- buffered saline (PBS), vortexed gently for 5 min, and serially diluted. 100 µL of each dilution was swabbed on Muller-Hinton Agar (MHA) medium plates. The plates were left at 37 ℃ for 24 hours, followed by colony enumeration. For the bacterial load determination, three independent wound tissue samples from each

group (n = 3 per group) were collected and processed in duplicate. Statistical analyses were performed using Microsoft Excel.

2.4.7. Pathological investigations

The samples were kept in 10% formalin for a full day after the skins of the treated and untreated mice were autopsied on the seventh day of the experiment and at the conclusion of the trial. Following a series of alcohol dilutions to dry them out, the samples were cleaned in xylene and then submerged in paraffin for an entire day in an oven (56 ℃). Tissue blocks with paraffin were sliced to an overall thickness of 5 μm by utilizing slide microtomes. Tissue specimens were removed, deparaffinized, and subjected to staining with Masson's trichrome, hematoxylin, and eosin (H&E) before being seen under a light microscope for histological examination [22,23]. Tissue sections from 3 mice per group (n = 3) were examined, and representative images are shown with scale bars. A blind histological examiner performed the pathological investigation.

Masson's trichrome staining:

Masson's trichrome staining and collagen quantification.

Masson's trichrome staining was performed on formalin-fixed, paraffin-embedded tissue sections according to a standard Masson's trichrome staining protocol. Briefly, tissue sections were deparaffinized in xylene and rehydrated through graded concentrations of ethanol to distilled water. Then, the sections were mordanted in Bouin's solution, followed by staining with Weigert's iron hematoxylin to visualize nuclei, Biebrich scarlet–acid fuchsin to stain cytoplasmic components, phosphomolybdic/phosphotungstic acid for differentiation, and aniline blue to selectively stain the collagen fibers. Following the staining procedure, sections were dehydrated through graded ethanol, cleared in xylene, and mounted for microscopic examination. In the ten highest intense staining at a high-power field, the Positive staining threshold was compared to the control cases. Collagen fibers were identified by their characteristic blue staining. Digital images of the stained sections were acquired under identical imaging conditions and analyzed using the ImageJ software. For a quantitative assessment, the images were subjected to color deconvolution to separate the blue collagen signal from the other staining components. Then, the collagen-positive area was segmented using an appropriate color threshold, and the percentage of collagen-positive area within the predefined region of interest (ROI) was calculated. The same image-acquisition and thresholding criteria were consistently applied to all experimental groups.

a. Histological scoring evaluates inflammation

The density and distribution of leukocytes were graded. A common multiparametric 4-point scale assessed the inflammatory cell infiltration per high-power field (HPF) on H&E-stained sections as follows [24]:

0: None (No observed inflammatory cells);

1: Mild/Rare (<25% of the wound bed/dermis affected);

2: Moderate (25%–50% of the wound bed/dermis affected); and

3: Severe/Marked (> 50% of the wound bed/dermis affected).

b. Scoring of vascular endothelial growth factor receptor (VEGF) in the skin

All immunostained slides were analyzed using a Zeiss microscope with high resolution (Axio Scope, Germany) in ten successive HPFs. Vascular endothelial growth factor (VEGF) antigens were expressed as brown cytoplasmic staining in Fibroblast-like cells and endothelial cells in the wound area, also in basal and supra-basal layers of the outer skin. VEGF antigens were assessed on a semiquantitative basis as the percentage of positively stained cells in 10 HPFs. Then, the means of percentages were calculated [25].

2.4.8. Pro- and anti-inflammatory cytokine detection

The enzyme-linked immunosorbent test (ELISA) was used. Three mice per group (n = 3) were randomly selected and euthanized at each time point (days 7 and 14 post-wounding). The original wound was 3 mm in diameter and was created using a biopsy punch. For the biochemical analysis, full-thickness tissue specimens were collected from the complete wound area together with a standardized 2-mm margin of the surrounding apparently healthy skin. The same sampling dimensions and procedure were applied to all animals to ensure comparable tissue collection among the experimental groups. Each sample was rinsed in ice-cold PBS and homogenized, and the resulting supernatant was stored at −80 ℃ until the cytokine analysis. To eliminate all blood, a little portion of the damaged skin was taken out, and the area was cleaned with ice-cold PBS (0.01 M and pH = 7.4). Using a glass homogenizer, pieces of frozen tissue were homogenized in PBS (1 g/9 mL); then, the homogenate was subjected to ultrasonic cell disruption (BioLogics, Inc., 150V/T, Virginia, USA) to further disintegrate the cells. Finally, the homogenate was centrifuged for 5 min at 5000 × g, and the resulting solution was preserved at −80 ℃ for later testing. Using a commercial ELISA kit (Elabscience, USA), the levels of human interleukin-6 (IL-6) and the human tumor necrosis factor-alpha (TNF-α) trimer cytokines were quantified. In short, following the addition of samples and standards to each well, biotinylated detection antibodies specific to both cytokines, along with an avidin-horseradish peroxidase (HRP) complex, were introduced, and the plates were then incubated. The optical densities of IL-6 and TNF-α were determined using biotinylated detection antibodies. The concentrations of the two cytokines were determined based on their respective OD values. Additionally, ELISA kits from BioSource International (Camarillo, California, USA) and commercially available reagents were used to measure the human interleukin-10 (IL-10) concentrations in mice. As directed by the manufacturer, the cytokine concentrations were measured by referencing a standard curve derived from the known concentration of cytokine standards provided on each assay plate [26,27]. The cytokine levels were measured in tissue homogenates from 3 mice per group (n = 3), with each sample assayed in duplicate.

2.5. In silico molecular docking studies

To elucidate the potential molecular mechanisms underlying the observed antibacterial and immunomodulatory activities of the *L. alte* extract, a comprehensive series of molecular docking simulations was conducted using the Autodock software suite.

2.5.1. Preparation of receptor structures

Molecular docking targets were selected based on the experimentally observed biological activities. DNA gyrase (from *S. aureus*) was chosen as the primary antibacterial target due to its essential role in bacterial DNA supercoiling and its status as a validated target for multiple antibiotic classes. For immunomodulatory effects, TNF-α, IL-6 (pro-inflammatory), and IL-10 (anti-inflammatory) were selected, as these cytokines showed statistically significant modulation (↓ TNF-α and IL-6; ↑ IL-10) in skin tissue following extract treatment, as determined by ELISA at days 7 and 14 post-wounding. The three-dimensional atomic coordinates of the four target proteins were retrieved from the RCSB Protein Data Bank (PDB). The selected targets were *Staphylococcus aureus* DNA gyrase complexed with DNA (PDB ID: 2XCT), TNF-α (PDB ID: 2AZ5), IL-6 (PDB ID: 1ALU), and IL-10 (PDB ID: 1Y6K). Prior to docking, all protein structures were meticulously prepared. All water molecules, co-crystallized ligands, ions, and any other non-essential heteroatoms were removed from the PDB files. Then, the structures were subjected to the Protonate 3D tool to add H atoms and assign appropriate ionization states at a simulated physiological pH of 7.4.

2.5.2. Preparation of ligand structures

The chemical structures of the twelve major compounds identified in the GC-MS analysis were constructed as 2D models using ChemDraw software. They were subsequently converted to 3D models and subjected to a rigorous energy minimization protocol using the Charm force field. The minimization was carried out until a root-mean-square gradient of <0.01 kcal/mol·Å was reached. This crucial step ensures that each ligand adopted a stable, low-energy conformation before being introduced to the protein's active site. Then, the database of minimized ligands was prepared for the docking procedure.

2.5.3. Docking simulation protocol

For each protein target, the active binding site was defined based on the location of the co-crystallized ligand in the original PDB file or identified using the Site Finder tool. Then, a docking simulation was performed for each of the twelve prepared ligands against each of the four protein targets. Next, the 30 best poses from this initial placement were subjected to refinement via forcefield energy minimization, allowing for flexible ligand-receptor interactions. The final poses were scored using the scoring function, which estimates the free energy of binding (B.E., in kcal/mol) of the ligand from a given pose. All 3D visualizations of the ligand-receptor complexes were generated using the built-in MOE visualizer and PyMOL (The PyMOL Molecular Graphics System, Version 2.0; Schrödinger, LLC). The binding energy (B.E.), root-mean-square deviation (rmsd), interaction energy (E_Int), and hydrogen bond energy (E_H_B) were tabulated for the comparative analysis.

2.6. Statistical data analysis

The software used to statistically analyze data was GraphPad Prism 9.0 (LLC). Tukey's post hoc test and one-way ANOVA were used to statistically compare the means. Data was provided in the form of mean ± standard deviation, with the threshold of significance set at less than 0.05.

3. Results

3.1. GC-MS results

The slug sample's GC-MS results revealed the existence of many chemicals with various biological functions. Table 1 listed the compounds' molecular formula, molecular weight, retention time (RT), area sum (%), compound class, and biological activity. Between these compounds are tris(2,4-di-tert-butylphenyl) phosphate, cholesterol, phenol, 2,4-bis(1,1-dimethylethyl)-, phosphite (3:1), and 7,9-Di-tert-butyl-1-oxaspiro (4,5) deca-6,9-diene-2,8-dione, with area sums of 44.42, 37.4, 7.97, and 2.59%, respectively.

Table 1. GC-MS analytical report of slug's extract.

Compound name	Molecular formula	Molecular weight	RT (min)	Area sum%	Compound class	Biological activity
1) Heptadecane, 2, 6, 10,15-tetra-methyl-	C21H44	296.6	23.419	0.54	Long-chain alkane	Metabolite observed in cancer metabolism. It has a role as a human metabolite [28]
2) 7,9-Di-tert-butyl-1-oxaspiro (4,5) deca-6, 9-diene-2, 8-dione	C17H24O3	276.4	25.669	2.59	α, β-unsaturated ketone	Pharmacological activities, including antineoplastic, antimicrobial and antiviral activities [29]
3) Stearic acid	C18H36O2	284.5	26.509	1.32	Long-chain fatty acid ethyl ester	antioxidants, hypocholesterolemic, nematicide, and pesticide [30]
4) 1-Octadecyne	C18H34	250.5	28.067	0.62	Straight chain alkyne	Antibacterial, antioxidant and anticancer [31]
5) 2-Pentadecyn-1-ol	C15H28O	224.3	28.118	0.81	Alcohol	
6) Octadecanoic acid, ethyl ester	C20H40O2	312.5	28.361	1.27	long-chain fatty acid ethyl ester	
7) 1,11-Dodecadiyne	C12H18	162.2	29.451	0.62	alkynes	
8) Oxirane, tetradecyl-	C16H32O	240.4	29.806	1.07	Epoxides	
9) 1,5,9Undecatriene, 2, 6,10-trimethyl-, (Z)-	C14H24	192.3	33.217	0.66	Terpens	
10) Cholesterol	C27H46O	386.7	35.328	37.4	Cholestanoid (sterol)	cardioprotective effect, anti-inflammatory, anticancer, antimicrobial, anti-psychotic, antioxidant activities and drug-delivery capability [32]
11) Phenol,2,4-bis(1,1-dimethylethyl)-, phosphite (3:1)	C42H63O3P	646.9	36.921	7.97	Phenols	antioxidant and anti-enterococcal properties [33]
12) Tris(2,4-di-tert-butylphenyl) phosphate	C42H63O4P	662.9	38.072	44.42	Aryl phosphate	Anti-inflammatory [34]

3.2. Analysis of the chemical profile of L. alte extract

The comprehensive chemical profiling of *L. alte* slug chloroform extract via GC-MS provides critical insights into its remarkable therapeutic potential, as demonstrated by this study. The identification of 12 distinct compounds (Table 1), dominated by four major constituents comprising >90% of the total detected area, established a robust chemical foundation for the observed bioactivities. This analysis examined the potential pharmacological relevance of these compounds in relation to the antibacterial and wound-healing activities observed in the present study. The GC-MS chromatogram revealed a chemically diverse profile, with several compounds possessing well-documented biological activities relevant to the study's findings:

Tris(2,4-di-tert-butylphenyl) phosphate (44.42%): This aryl phosphate ester was the most abundant compound. While direct studies on its biological activity are limited, structural analogues and related organophosphates demonstrate significant anti-inflammatory properties [34]. Its high abundance strongly correlated with the *in vivo* observation of drastically reduced pro-inflammatory cytokines (IL-6 and TNF-α) and accelerated wound closure.

Cholesterol (37.4%): The high concentration of this ubiquitous sterol was particularly noteworthy. Beyond its structural role in membranes, cholesterol possesses documented anti-inflammatory, antimicrobial, and wound-healing-promoting activities [32]. Its presence may be involved in membrane stabilization and enhancing skin barrier repair in the proliferative phase, precursor function, which serves as a precursor for vitamin D synthesis (promoting keratinocyte differentiation) and steroid hormones involved in inflammation resolution, and growth factor modulation, that influences signaling pathways crucial for cell migration and angiogenesis.

Phenol, 2,4-bis(1,1-dimethylethyl)-, phosphite (3:1) (7.97%): This phenolic antioxidant belongs to a class known for radical scavenging and anti-enterococcal properties [33]. Its role is crucial in mitigating oxidative stress at the wound site, which is a major impediment to healing [35]. By neutralizing reactive oxygen species (ROS) generated during inflammation, it protects cells and matrix components, thereby facilitating a transition to the proliferative phase. Its antioxidant capacity complements the anti-inflammatory action of the dominant aryl phosphate.

7,9-Di-tert-butyl-1-oxaspiro(4,5)deca-6,9-diene-2,8-dione (2.59%): This α,β-unsaturated ketone/spiro compound, though present in a smaller proportion, exhibited potent predicted antibacterial activity.

The extract contained several minor components (<2% each) known for diverse bioactivities. Stearic acid (1.32%) and Octadecanoic acid, and Ethyl Ester (1.27%): These long-chain fatty acids/esters possess reported antioxidant, hypocholesterolemic, and antimicrobial activities [30,36]. 1-Octadecyne (0.62%): This alkyne has documented antibacterial, antioxidant, and anti-cancer properties [31]. Heptadecane derivatives, Terpenes (e.g., 1,5,9-Undecatriene,2,6,10-trimethyl-,(Z)-), and Epoxides: While their specific contributions require further study, these classes often exhibit antimicrobial or anti-inflammatory effects, which may potentially contribute to the overall biological activity of the crude extract, but the specific contribution of each constituent is yet to be experimentally determined. The chemical profile of *L. alte* extract revealed a significant novelty, where the high abundance of Tris(2,4-di-tert-butylphenyl) phosphate in the molluskan therapeutic extract was unusual and highlighted its potential as an anti-inflammatory compound. The occurrence of cholesterol, together with phenolic and potentially antimicrobial constituents (Oxaspiro compound), differs from profiles reported in other snail/slug mucins or extracts, which generally emphasize proteins, peptides,

glycosaminoglycans, and hyaluronic acid [13,37,38]. This chloroform extract targets a distinct, lipid-soluble chemical space [39,40]. The study bridges traditional knowledge (use of slugs) with modern analytical (GC-MS) and computational (docking) techniques, thus providing mechanistic hypotheses for the observed efficacy.

3.3. In vitro assessment of the slug extract's antibacterial activity against Staphylococcus aureus

3.3.1. MIC determination

The *in vitro* antibacterial activity of the *L. alte* chloroform extract was quantitatively assessed against the bacterium *S. aureus* ATCC 6538 using a broth microdilution assay. The extract exhibited a clear dose-dependent inhibitory effect on the growth of *S. aureus*. A MIC value of 0.625 mg/mL was determined. This value represents the lowest concentration of the extract that completely inhibits the visible growth of the bacteria after 24 hours of incubation at 37 ℃. As illustrated in the dose-response curve (Figure 1), a progressive reduction in bacterial cell viability was observed with increasing concentrations of the slug extract, with viability dropping from 100% in the untreated control to near-zero levels at and above the determined MIC. This confirmed the potent antibacterial efficacy of the crude extract against this bacterial strain.

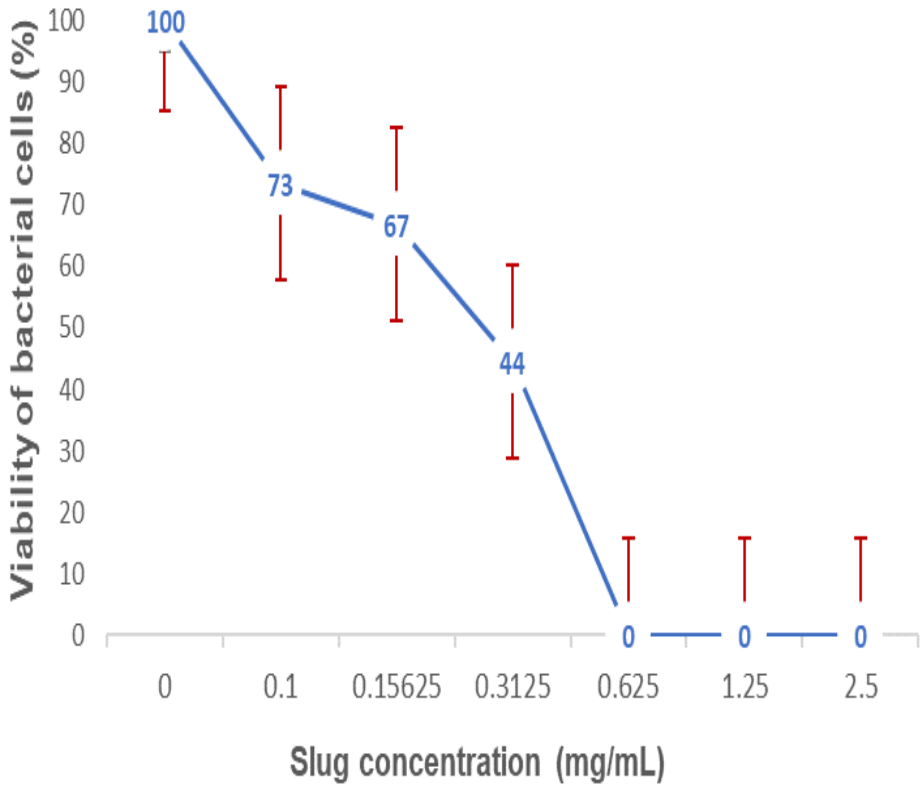


Figure 1. Slug's MIC and antibacterial efficacy against *S. aureus* ATCC 6538. The obtained results were shown as the average (n = 3) and standard error bars represent ± 5%.

3.4. In-Silico docking interaction

3.4.1. *In Silico* docking analysis against *S. aureus* DNA gyrase

Molecular docking provided hypothetical binding modes and affinity estimates; these computational predictions require experimental validation through biophysical assays (e.g., surface plasmon resonance (SPR), isothermal titration calorimetry (ITC)) and functional studies to confirm actual target engagement and inhibition. All twelve major compounds identified via GC-MS were docked into the active site of the *S. aureus* DNA gyrase-DNA complex (PDB ID: 2XCT [39]), a validated target for antibacterial agents. The docking scores, including the B.E., E_Int, and E_H_B, were presented in Figure 2. The study targeted the bacterial DNA gyrase, a type II topoisomerase that is essential for bacterial survival but absent in humans, making it an ideal and well-established target for antibacterial drugs, most notably the fluoroquinolone class [41]. DNA gyrase is responsible for introducing negative supercoils into DNA, a process critical for relieving torsional stress during DNA replication and transcription. Its inhibition leads to the disruption of these vital processes and ultimately results in bacterial cell death [42]. The results suggested that several compounds from the extract exhibited strong predicted binding affinities for the DNA gyrase active site, with binding energies ranging from −5.203 to −7.523 kcal/mol. Notably, the organophosphorus compounds phenol,2,4-bis(1,1-dimethylethyl)-, phosphite (3:1) (compound 11) and tris(2,4-di-tert-butylphenyl) phosphate (compound 12) emerged as the most potent binders, with binding energies of −7.523 kcal/mol and −7.509 kcal/mol, respectively. Moreover, these compounds demonstrated the most favourable interaction energies (−32.540 kcal/mol and −21.436 kcal/mol, respectively), possibly indicating extensive and stable non-covalent interactions within the binding pocket. Other compounds also showed significant binding potential. Cholesterol (compound 10) and octadecanoic acid, ethyl ester (compound 6) displayed strong binding energies of −6.924 kcal/mol and −6.852 kcal/mol, respectively. Of note, compound 6 exhibited an exceptionally low RMSD value of 1.009 Å, suggesting a highly stable and well-defined binding pose. Visual inspection of the docking poses for the top three binders revealed key molecular interactions responsible for their high affinity (Figure 2). All three compounds positioned themselves within the enzyme's active site, interacting with key catalytic residues and the bound DNA. A critical interaction was observed with the residue arginine 458 (Arg458), as well as with the DNA bases deoxyguanosine 9 (DG9) and adenine 13 (A13). The bulky, hydrophobic tert-butyl groups of compounds 11 and 12 were stabilized by hydrophobic contacts within the pocket, while their phosphate/phosphite moieties formed strong hydrogen bonds and electrostatic interactions with the positively charged guanidinium group of Arg458. Similarly, the hydroxyl group of cholesterol (10) acted as a hydrogen bond donor/acceptor, while its rigid sterol backbone was anchored by extensive van der Waals forces and hydrophobic interactions with the active site and DNA backbone. These interactions may effectively anchor the ligands in the active site, suggesting a potential mechanism for enzyme inhibition.

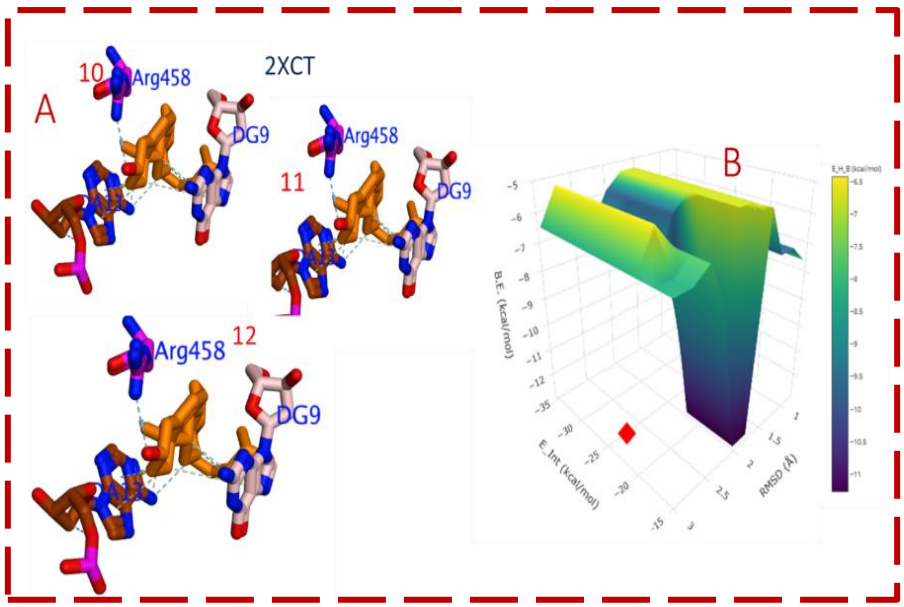


Figure 2. (A) Docking poses of the top three binding (10–12) compounds from *L. alte* extract within the active site of *S. aureus* DNA gyrase (PDB: 2XCT). Dashed lines represent non-covalent interactions such as hydrogen bonds and hydrophobic contacts. (B) Molecular docking scores including the B.E. (Binding Energy), rmsd (Root Mean Square Deviation), E_Int (Interaction Energy), and E_H_B (Hydrogen Bond Energy). All energy values are in kcal/mol.

3.5. The impact of slug extract on wound healing and its antibacterial efficacy against S. aureus in vivo

3.5.1. Estimation of wound size at the macroscopic level

The application of slug extract enhanced and accelerated the process of wound healing, as shown in Figure 3A, as after 14 days, the wound was completely healed after treatment with slug extract. Additionally, the induction of slug extract could accelerate the healing process after 14 days (Figure 3A). The healing percentage didn't show significant changes after 7 days of treatment (Figure 3B1), while the healing process was accelerated in the slug treated group with 84.4 healing percentage after 14 days of treatment as compared with the negative group that showed 41.1 healing percentage (Figure 3B2).

3.5.2. Bacterial load determination

After seven days of wound therapy, the bacterial content in the tissue that received slug extract was the least compared with that within the tissues of the positive and negative controls, as illustrated in Figure 4. On day zero, the total bacterial count was $4 \times 10^4 \pm 1.41$ CFU/mL ($3 \times 10^4 \pm 1.414$, $5 \times 10^4 \pm 1.414$, and $4 \times 10^4 \pm 1.414$), but after seven days of the experiment, the total count was uncountable, $16 \times 10^2 \pm 3.3$ ($15 \times 10^2 \pm 4.24$, $17 \times 10^2 \pm 1.41$, and $16 \times 10^2 \pm 4.24$), and $5 \times 10^2 \pm 1.89$ ($4 \times 10^2 \pm 1.41$, $6 \times 10^2 \pm 2.83$, and $5 \times 10^2 \pm 1.41$) CFU/mL in the wounded tissues of the negative control (group I), positive control (group II), and treated with slug (group III), respectively.

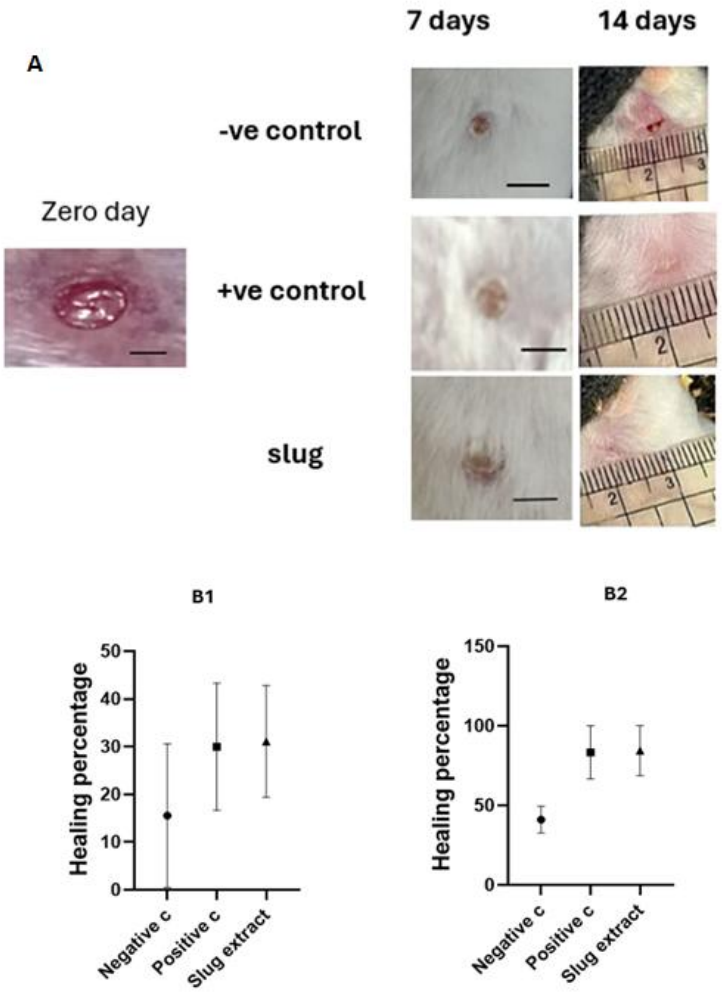


Figure 3. The effect of slug administration on the healing of *S. aureus*-infected wounds after 7 and 14 days (A). After 7 days, no significant changes (P = 0.035) in the healing percentage were observed between the treated and control groups (B1). However, after 14 days, significant changes ($P < 0.05$) were observed between the two groups (B2). A one-way ANOVA was used (n = 3).

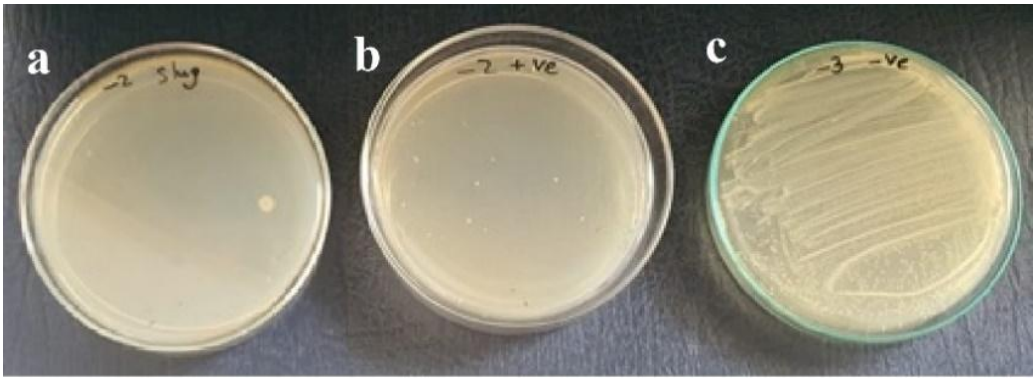


Figure 4. Bacterial load in wounded tissues after 7 days of *in vivo* experiment a) treated with slug, b) positive control, and c) negative control.

3.6. Histological investigations

According to the current findings, a skin segment from a normal mouse showed a typical structure, with an intact epidermis made up of two to three cell layers, followed by a layer of dermal connective tissue that contained hair follicles and sebaceous glands (Figure 5A). VEGF was moderately expressed in the cytoplasmic stain of the epidermis and dermis blood vessels in the sections of normal mice (immunohistochemistry, VEGF, DAB) (Figure 5B). Numerous polymorpho-nuclear neutrophils and lymphocytes infiltrated the epidermis and dermis of the mice's skin sections with positive injuries, causing ulcer formation and indicating the presence of inflammatory cells. Furthermore, hair follicles and sebaceous glands were seen (Figure 5C). Likewise, the cytoplasmic staining of epidermal and dermis blood vessels revealed moderate to substantial expression of VEGF (Figure 5D). Skin slices from the injured mice showed a healed lesion with intact epidermis and dermis after seven days of slug extract treatment. Sebaceous glands and hair follicles were not present in the healed ulcerated area, but polymorphonuclear neutrophils and lymphocytes moderately infiltrated the epidermis and dermis, indicating the existence of inflammatory cells (Figure 5E). Additionally, VEGF was mildly expressed in the blood vessels of the epidermis and dermis, as indicated by cytoplasmic staining (Figure 5F). Following 14 days of slug extract treatment, skin slices from the injured mice revealed an unbroken epidermis and a healed ulcer. A healed ulcer showed modest infiltration of neutrophils, lymphocytes, and inflammatory cells into the epidermis and dermis, along with degeneration of the sebaceous glands and hair follicles (Figure 5G). Additionally, VEGF was moderately expressed in the blood vessels of the epidermis and dermis, as indicated by cytoplasmic staining (Figure 5H).

3.6.1. Histological analysis and collagen quantification

Using the ImageJ digital color deconvolution for the quantitative analysis of architectural matrix remodeling, a high variability of collagen deposition was observed among the experimental groups (Figure 6). Across the treatment groups, the staining methods generally showed a trend of increased collagen density compared to the control group. The staining methods can digitally quantify the collagen density in wound healing research (Table 2). The baseline area percentage of the normal/reference skin was 0.484%. In contrast, the quantified pixel percentage within the negative control (untreated ulcer) group showed a significant localized increase to 11.875% ($p < 0.05$ vs. normal/reference skin) (Table 2). This finding is indicative of a dense but highly disordered fibroblastic response characteristic of unresolved wound architecture. In the trial, topical administration of the slug extract *Laevicaulis alte* significantly controlled the tissue rearrangement and promoted a progressive matrix alignment. These results indicate that the structural collagen density transitioned from an intermediate of 2.239% at day 7 to a more ordered assembly of 3.824% by day 14 ($p < 0.05$ vs. Negative Control) because of the active deposition of extracellular matrix and healthy transition into the advanced remodeling phase of wound healing.

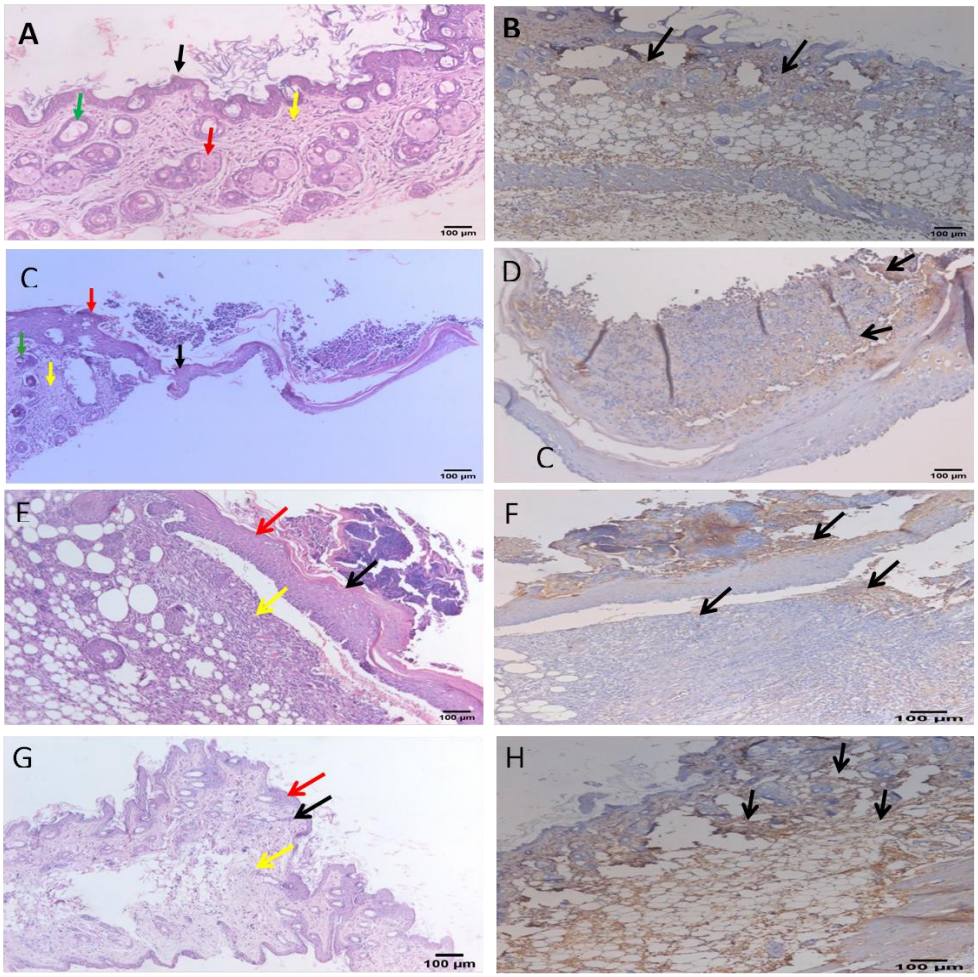


Figure 5. Skin sections from mice. A) A skin section from normal reference skin exhibited normal skin, intact epidermis formed of 2–3 cell layers) (black arrow), dermis (connective tissue) (yellow arrow), sebaceous glands (red arrow), and hair follicles (green arrow), (piliary canals), (H&E). B) Showed moderate expression of VEGF as cytoplasmic stain in epidermis and dermis blood vessels (Immunohistochemistry, VEGF, DAB). C) A skin section from the injured mice in the positive control group displayed ulcer formation (black arrow), with nearby regions exhibiting normal skin distinguished by an epidermis formed of 2–3 cell layers) (red arrow), underlying with connective tissue (yellow arrow) and hair follicles (green arrow). Within the ulcerated region, infiltration of numerous polymorph neutrophils and lymphocytes into both the epidermis and dermis was evident (red head arrows), along with sebaceous glands and hair follicles (green arrow) (H&E). D) Showed moderate- marked expression of VEGF as a cytoplasmic stain in the epidermis and dermis blood vessels (black arrow) (Immunohistochemistry, VEGF, DAB). E) A skin section from the treated group with slug mucin after 7 days showed healed ulcer (black arrow), intact epidermis (formed of 2–3 cell layers) (red arrow), dermis (layer of connective tissue) (yellow arrow), Healed ulcerated area, showed moderate infiltration of inflammatory cells, neutrophils, lymphocytes, and polymorphs into the epidermis and dermis; lack of sebaceous glands and hair follicles (H&E). F) Showed mild expression of VEGF as a cytoplasmic stain in the epidermis and dermis blood vessels (black arrow)

(Immunohistochemistry, VEGF, DAB). G) A skin section from the treated group with slug mucin for 14 days showed a healed ulcer (black arrow) and an intact epidermis (external epithelium formed of 2–3 cell layers) (red arrow). The healed ulcerated area showed mild infiltration of the epidermis and dermis by polymorph, neutrophils, and lymphocytes inflammatory cells (yellow arrows), degenerated of both sebaceous glands and hair follicles (black arrow) (H&E). H) Exhibited moderate expression of VEGF as cytoplasmic stain in the epidermis and dermis blood vessels (Immunohistochemistry, VEGF, DAB). Scale bar is 100 µm.

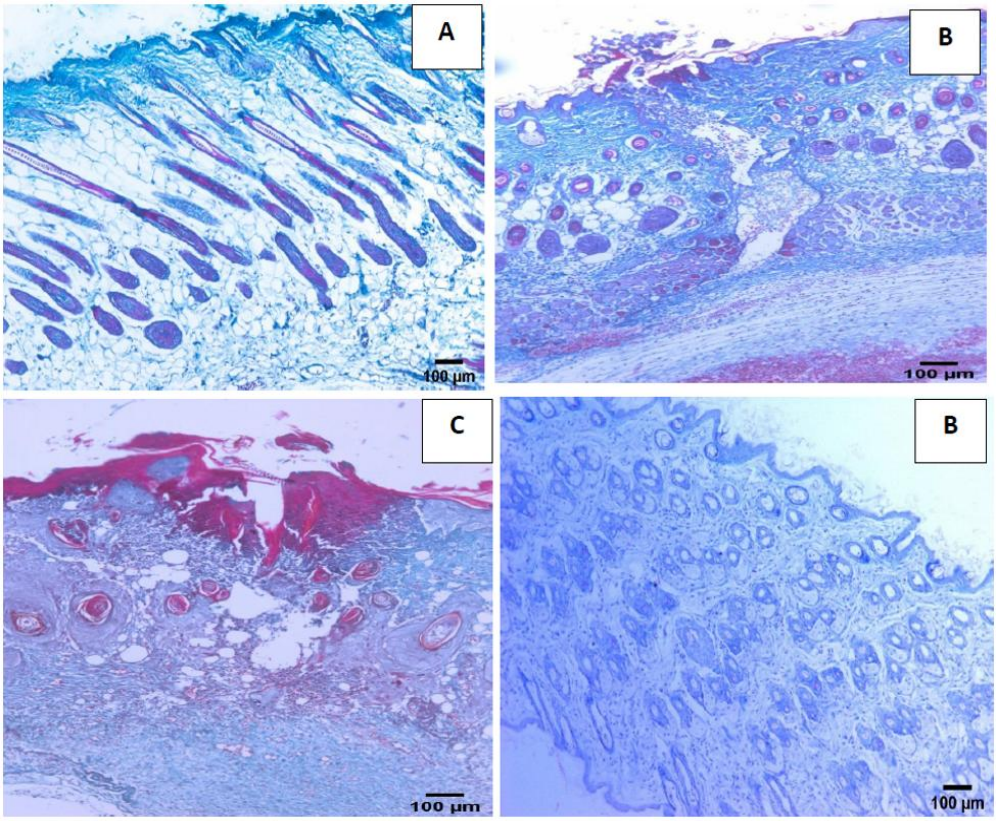


Figure 6. Masson's trichrome stain section. A) A skin section from normal/reference skin, few disorganized collagen, and fibroblastic proliferation. B) Showing large amount of collagen deposition. C) Mild amount of collagen deposition. D) Mild amount of collagen deposition. Scale bar is 100 µm.

Table 2. Digital quantification of tissue section collagen fibers via ImageJ (color deconvolution).

Experimental group label	Total area evaluated	Median grey value	Collagen density (%Area)	Statistical significance
normal/reference skin	234,498	200	0.484%	–
Negative Control	234,498	182	11.875%	$p < 0.05$ vs. normal/reference skin
Treated 7 Days	234,498	224	2.239%	$p < 0.05$ vs. Negative Control
Treated 14 Days	234,498	236	3.824%	$p < 0.05$ vs. Negative Control

3.6.2. Semiquantitative histological evaluation of inflammation

A semi-quantitative evaluation of leukocyte infiltration in H&E-stained tissue sections showed a clear pattern of resolution of the inflammatory phase after treatment (Table 3). The normal/reference skin group showed the baseline tissue architecture with inflammatory cell score as 1 (mild). Contrastingly, the negative control (ulcer) untreated group showed severe and pronounced active leukocyte infiltration, receiving the maximum score of 3, indicating that more than 50% of the wound bed and dermal layers were still heavily compromised by an ongoing inflammatory response. The topical administration of the extract of the slug led to a progressive and well-controlled diminution of this inflammatory influx. On day 7 of treatment, there was a moderate tissue transition with an inflammatory score of 2. By day 14, the infiltration score had dropped to 1, indicating near complete resolution of the active phase of inflammation and return to baseline levels, supporting the progressive healing and tissue-regenerative properties of the extract.

Table 3. Semi-quantitative scoring of inflammatory cell infiltration (H&E stain).

Experimental group	Inflammatory score (0–3)	Pathological presentation
Normal/reference skin	1	Mild/Rare inflammatory cells; normal baseline skin tissue architecture.
Negative Control	3	Severe/Marked active leukocyte infiltration affecting >50% of the dermis.
Treated 7 days	2	Moderate infiltration (25%–50% of the wound bed affected), showing a localized healing transition.
Treated 14 days	1	Mild/Rare inflammatory cells, indicating complete or near-complete resolution of inflammation.

7 days after the incision: Infiltration of mononuclear and polymorphonuclear leukocytes and fibroblast-like cells expressing VEGF are seen in the wound area (Figure 7).

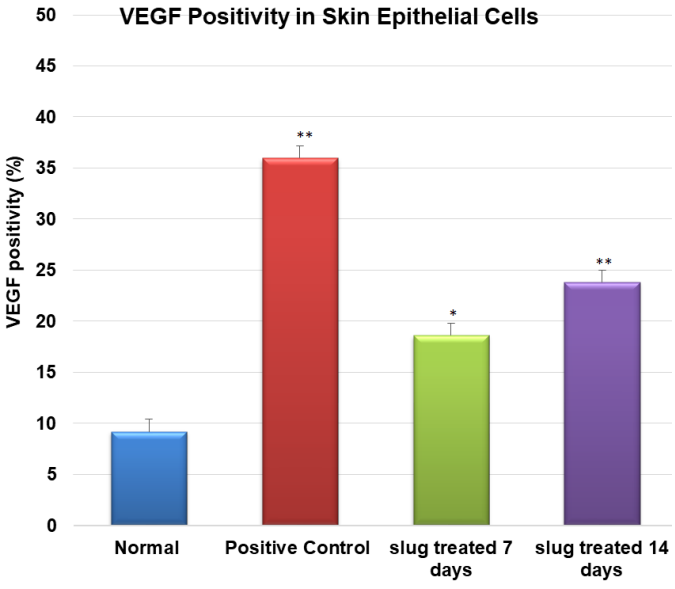


Figure 7. Vascular endothelial growth factor (VEGF) positivity percentage.

14 days after the skin incision: Fibroblast-like cells and endothelial cells express VEGF in the wound area. Intact skin area shows positive VEGF in skin epithelial cells (basal and supra basal layers of the outer skin surrounding ulcer), which showed no change during the wound process (Figure 7).

3.7. Pro-and anti-inflammatory cytokines detection

The slug extract showed a promising effect on both the pro-inflammatory and the anti-inflammatory cytokines in the wound of the skin of mice. There was a significant decrease in the pro-inflammatory cytokines represented by IL-6 and TNF-α levels after 7 and 14 days of slug extract treatment as compared with the negative control group. Conversely, the anti-inflammatory biomarker IL-10 levels were significantly increased as compared with the negative controls after treating with the slug extract on 7 and 14 days' post-wound (Figure 8).

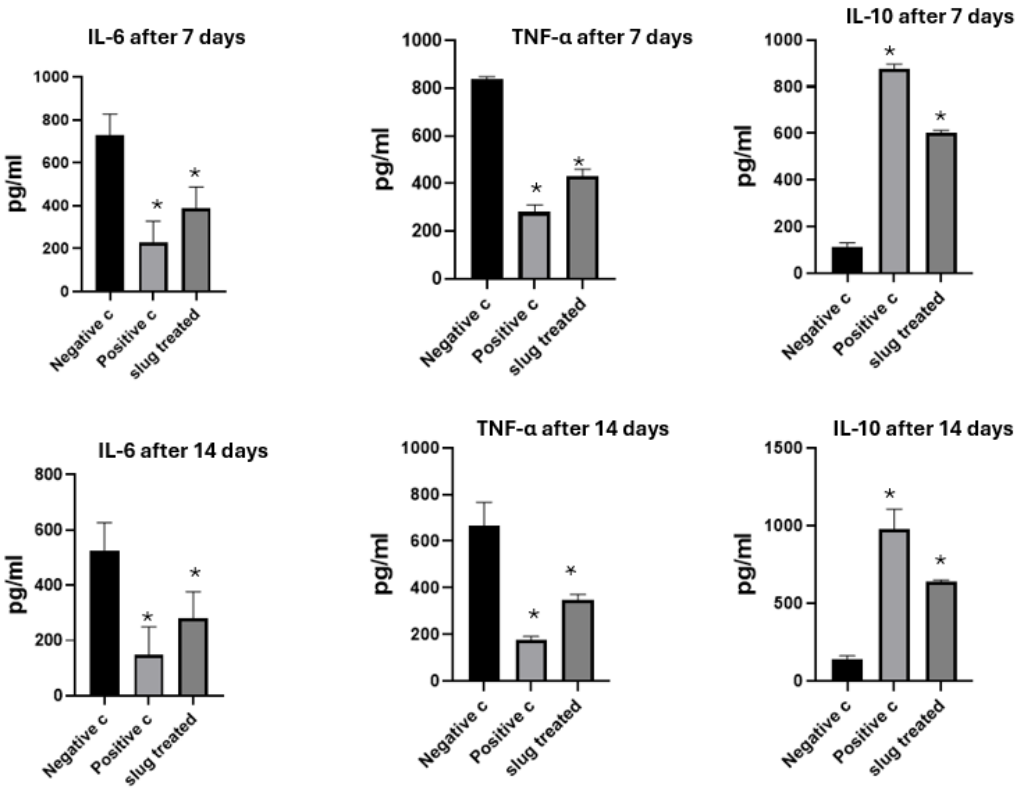


Figure 8. Proinflammatory cytokine levels (IL-6 and TNF-α) and anti-inflammatory cytokine level (Il-10) after treatment with slug extract after 7 and 14 days. All values represent (mean ± SD). *Significant ($P < 0.05$) on compared with the negative control.

3.8. In-Silico docking interaction results

To investigate the molecular mechanisms underlying the observed immunomodulatory activity of the *L. alte* extract, a comprehensive molecular docking study was performed. The twelve major compounds identified by GC-MS were docked against the binding sites of three key cytokines: The pro-inflammatory mediators including TNF-α (PDB: 2AZ5 (43)), IL-6 (PDB: 1ALU (44)), and the

anti-inflammatory cytokine IL-10 (PDB: 1Y6K (45)). The binding affinities and interaction parameters were represented in Figures 9–11. The docking results revealed that the compounds from the slug extract, particularly the organophosphorus derivatives and cholesterol, exhibited significant and differential binding affinities for the cytokine targets.

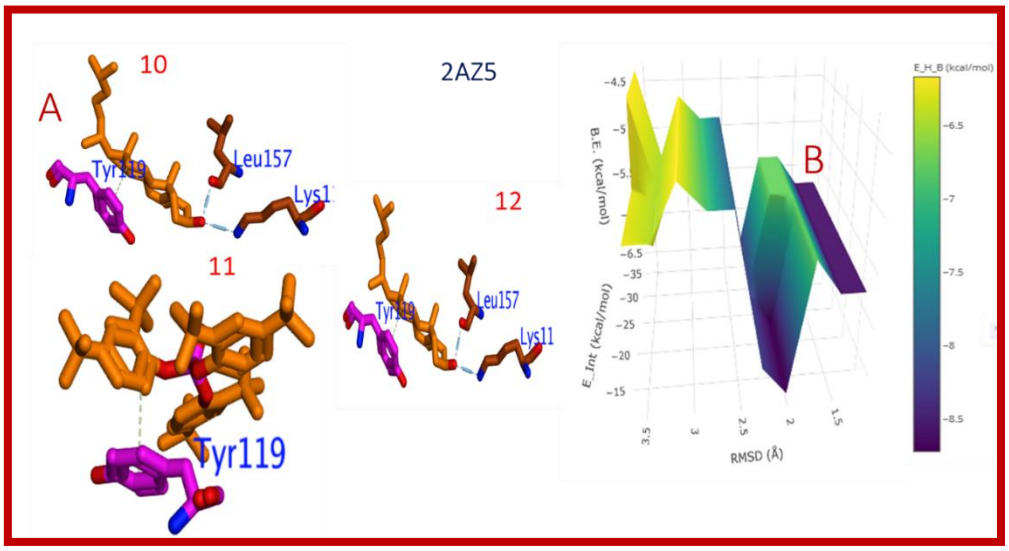


Figure 9. (A) Docking poses of the top three binding (10–12) compounds from *L. alte* extract within the active site of TNF-α (PDB: 2AZ5). Dashed lines represent non-covalent interactions such as hydrogen bonds and hydrophobic contacts. (B) Molecular docking scores including the B.E. (Binding Energy), rmsd (Root Mean Square Deviation), E_Int (Interaction Energy), and E_H_B (Hydrogen Bond Energy). All energy values are in kcal/mol.

3.8.1. Interaction with pro-inflammatory cytokines

TNF-α (PDB: 2AZ5): The strongest predicted binding affinity was observed for compound (11), with a B.E. of −6.663 kcal/mol. This was closely followed by tris(2,4-di-tert-butylphenyl) phosphate (12) and cholesterol (10) with B.E. values of −6.373 kcal/mol and −5.693 kcal/mol, respectively. A visual analysis of the binding poses (Figure 9) revealed that compound 11 engaged in a crucial π-stacking interaction with the aromatic ring of Tyr119. Compounds 10 and 12 were stabilized by H-bonds with the backbone of Leu157 and electrostatic interactions with Lys11. IL-6 (PDB: 1ALU): The binding affinities for IL-6 were generally more modest. The most favorable interaction was for tris(2,4-di-tert-butylphenyl) phosphate (12), with a B.E. of −5.163 kcal/mol. The interactions, shown in Figure 10, were primarily driven by π-π stacking with the indole ring of Trp157 and hydrophobic contacts with Gln156. Cholesterol (10) formed a key hydrogen bond with the side chain of Lys46. Complete docking score table for all compounds are found in Table S1.

3.8.2. Interaction with anti-inflammatory cytokine

IL-10 (PDB: 1Y6K): The slug compounds demonstrated the strongest overall binding affinities for the anti-inflammatory cytokine IL-10. Compounds 12 and 11 emerged as the most potent binders, with excellent B.E. values of −7.433 kcal/mol and −7.188 kcal/mol, respectively. Cholesterol (10) also

showed a strong affinity with a B.E. of −5.997 kcal/mol. The binding modes for compounds 11 and 12 were stabilized by extensive hydrophobic interactions with the aromatic ring of Phe37 (Figure 11). Collectively, these results indicated that the lead compounds from the slug extract, particularly 9, 10, and 11, have the structural capacity to effectively interact with both pro- and anti-inflammatory cytokine targets through distinct molecular interactions.

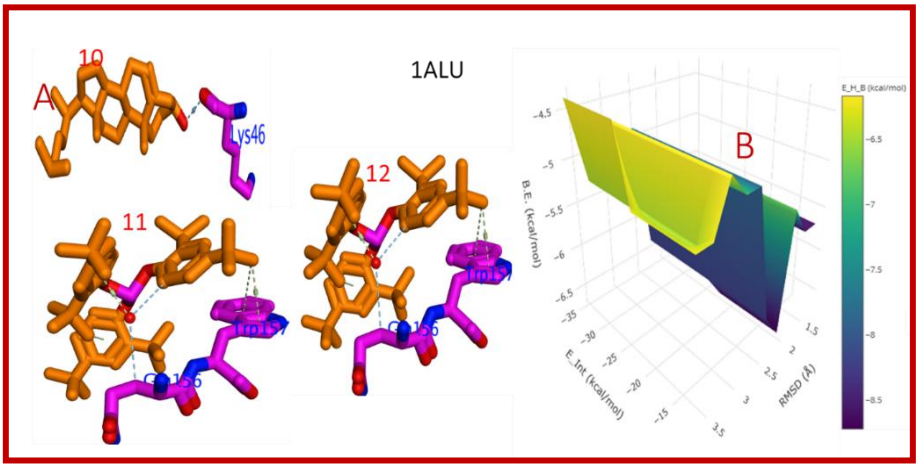


Figure 10. (A) Docking poses of the top three binding (10–12) compounds from *L. alte* extract within the active site of IL-6 (PDB: 1ALU). Dashed lines represent non-covalent interactions such as hydrogen bonds and hydrophobic contacts. (B) Molecular docking scores including the B.E. (Binding Energy), rmsd (Root Mean Square Deviation), E_Int (Interaction Energy), and E_H_B (Hydrogen Bond Energy). All energy values are in kcal/mol.

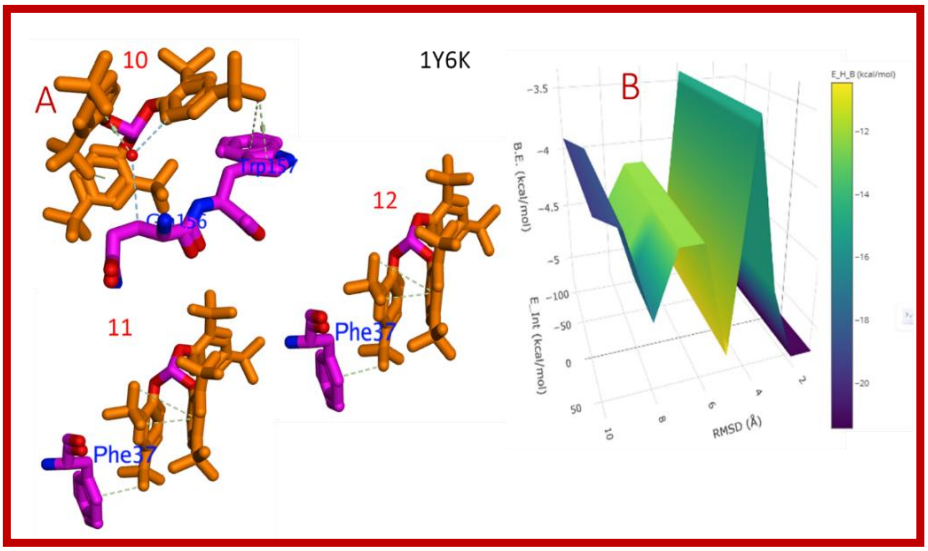


Figure 11. (A) Docking poses of the top three binding (10–12) compounds from *L. alte* extract within the active site of IL-10 (PDB: 1Y6K). Dashed lines represent non-covalent interactions such as hydrogen bonds and hydrophobic contacts. (B) Molecular docking scores including the B.E. (Binding Energy), rmsd (Root Mean Square Deviation), E_Int (Interaction Energy), and E_H_B (Hydrogen Bond Energy). All energy values are in kcal/mol.

4. Discussions

Antibiotic efficacy is reduced or even lost due to the current load of multidrug resistance and the emergence of superbugs, which presents serious difficulties in the treatment of infectious diseases. Due to the issues surrounding the decline and even loss of antibiotic efficacy brought on by a growth in bacterial resistance, there is currently a major need to discover new antibiotics that are both safe and effective for society. Antibiotics are connected to adverse side effects even though they are useful in treating and preventing diseases in both humans and animals [46]. The treatment of bacterial infections and associated co-morbidities is seriously hampered by the rise of extensively and multi-drug-resistant pathogens. Conventional treatments are gradually losing their efficacy due to the alarming rise and extensive spread of antibiotic resistance as well as the development of new antibiotics [47]. Therefore, searching for new, unconventional sources that have an antibacterial effect has become important nowadays. Although snails and slugs perform multifunctional roles through the regulation of algae and fungi, endozoochory, litter decomposition, facilitation of nutrient recycling, and by being prey to various invertebrates and vertebrates, snails and slugs are very destructive pests that eat the twigs of plants and crops, which hurts the economy [48]. To avoid serious harm from *Laevicaulis alte* slugs, in this study, we used the roasted form of them as an antibacterial agent against *Staphylococcus aureus in vitro* and *in vivo*. The obtained results indicated *in vitro* reduction of the *Staphylococcus aureus* cell density with an MIC value of 0.625 mg/mL. Additionally, the number of bacteria (bacterial load) was reduced during the *in vivo* trial, especially in the wounded tissue that was treated with slug compared with negative and positive controls. Generally, insects such as snails and slugs make slime, which is a mucus-like substance with a complex makeup. 90% to 99.7% of snail and slug slime is water, with the remaining 0.3% to 10% being made up of enzymes, glycoproteins, proteoglycans such as hyaluronic acid, achacin, glycosaminoglycans, antimicrobial peptides, copper peptides, and metal ions [13]. Moreover, thousands of bioactive compounds, including polypropionate, terpenes, sterols, fatty acid derivatives, alkaloids, and nitrogenous substances, have been discovered to be present in mollusks. The antibacterial, cytotoxic, antitumor, anti-inflammatory, antileukemic, antineoplastic, and antiviral qualities of these substances in mollusks have been the subject of much research [38].

According to the GC/MS results, the current investigation showed that the slug extract included 12 different chemicals, including phenols, terpenes, cholesterol, and fatty acids. The current data were similar to findings of Ibrahim et al. [37], who reported that GC/MS examination of *E. desertorum* mucin resulted in ten compounds have been identified, which were mainly quinolines, monoterpenes, alcohol esters, sesquiterpenoids, fatty acid esters, fatty acids, and phenol derivatives. Sallam et al. [49] reported that such compounds have antimicrobial, anticancer and antioxidant activities. The GC-MS analysis of the slug extract revealed several compounds with diverse biological functions. Between these were the following compounds: Tris (2,4-di-tert-butylphenyl) phosphate, cholesterol, phenol,2,4-bis(1,1-dimethylethyl)-,phosphite (3:1), and 7,9-Di-tert-butyl-1-oxaspiro(4,5)deca-6,9-diene-2,8-dione, with area sums of 44.42, 37.4, 7.97, and 2.59%, respectively. The GC-MS analysis of *L. alte* extract was not merely a compositional list; it was the key to understanding its remarkable therapeutic potential. The profile revealed a sophisticated blend of bioactive lipids and phenolics, dominated by anti-inflammatory (tris(2,4-di-tert-butylphenyl) phosphate, cholesterol), antioxidant (phenol derivative), and antimicrobial (7,9-Di-tert-butyl-1-oxaspiro (4,5) deca-6,9-diene-2,8-dione, fatty acids) compounds.

In silico docking provided plausible molecular targets for these activities, corroborating the *in vitro* and *in vivo* results. The presence of multiple constituents with potentially relevant antibacterial,

anti-inflammatory, and antioxidant properties may collectively contribute to the biological effects observed against *S. aureus* infection and during wound repair leading to complete wound closure within 14 days. However, the relative contribution of individual constituents and their potential interactions cannot be determined from the present study. This chemical blueprint positions the *L. alte* slug extract as a highly promising natural source for developing novel therapeutic agents targeting infected and chronic wounds. Future research should focus on isolating the major active principles (particularly the aryl phosphate and oxaspiro compound), validating their individual and combined efficacies, and exploring formulation strategies for topical delivery. The docking results suggested that multiple components of the slug extract can effectively occupy and interact with the enzyme's active site. The two most potent compounds, 12 and 11, displayed the highest predicted affinity. Their efficacy was likely derived from a combination of structural features. The bulky, lipophilic tert-butylphenyl groups can engage in extensive hydrophobic and van der Waals interactions within the binding pocket, while the central phosphate/phosphite group provided a critical anchor point. As seen in Figure 2, this polar moiety formed strong electrostatic interactions and H-bonds with Arg458. The positively charged guanidinium group of arginine residues was frequently involved in stabilizing the negatively charged phosphate backbone of DNA or interacting with small molecule inhibitors, making this interaction particularly significant for potent inhibition [50]. The strong binding of cholesterol (10) and ethyl ester of octadecanoic acid (6) further reinforced the hypothesis that multiple constituents of the crude extract may contribute to its overall biological activity. While their binding energies were slightly less favorable than the top two organophosphates, their relatively high abundance suggested that they may contribute to the overall biological activity of the extract; however, their individual contributions require experimental validation. Cholesterol's rigid, hydrophobic structure is well-suited to occupy hydrophobic pockets, while its single OH group provided a specific H-bonding capacity. Likewise, the long aliphatic chain of octadecanoic acid provided hydrophobic anchoring. The remarkably low RMSD of compound 6 suggested a particularly favorable and conformationally locked binding mode, which is often indicative of a high-affinity interaction. It was crucial to interpret these findings in the context of the whole extract. The observed MIC of 0.625 mg/mL reflected the antibacterial activity of the crude extract, which contains multiple chemical constituents. The relative contribution of individual compounds to the observed activity remains to be established. The predicted interactions of several constituents with the bacterial target suggest that multiple compounds within the crude extract may interact with the enzyme through distinct binding modes. The presence of multiple bioactive constituents may represent a potential advantage of crude natural extracts; however, whether these constituents act independently, additively, or synergistically requires dedicated experimental evaluation [51]. Additionally, this approach can be a strategy to circumvent the development of drug resistance, as it is more difficult for a bacterium to simultaneously evolve resistance mechanisms against multiple active molecules. However, we caution that these computational predictions cannot demonstrate functional cytokine modulation or establish causal relationships with the observed *in vivo* effects.

For medical applications, it is crucial to explore the possibility of discovering novel, potent bioactive compounds that can quicken wound healing by decreasing tissue fibrosis, re-epithelialization, and wound closure time. Cutaneous wound healing is a complex biological process. Restoring the injured epithelium's barrier function necessitates the synchronization of time and spatially regulated cellular and molecular activities [20]. The histological sections of the wounded skin from the treated group with slug extract demonstrated a recovered ulcer with slight infiltration of polymorphonuclear leukocytes, neutrophils, and lymphocytes in the epidermis and dermis. Sebaceous glands and hair follicles were absent, while the epidermis and dermis remained intact. Similar outcomes were obtained

by El-Sayed et al. [19], who found that selenium nanoparticles could heal the wound after 11 days. Additionally, Errajouani et al. [52] showed that slime from the garden snail *Cepaea hortensis* helped almost completely heal excision wounds in rabbits after 24 days of treatment. The inflammatory phase is the most crucial stage in the healing process for wounds. Moreover, persistent inflammation results in significant healing disruptions, an increase in fibrosis and scarring, and elevated levels of cytokines, including IL-6, TNF-α, and IL-1. TNF-α is a cytokine that induces inflammation and is expressed at high levels during inflammation [35]. Moreover, the multipurpose cytokine IL-6 influences inflammation, haematopoiesis, and immune responses in pleiotropic ways [40]. The current study demonstrated that slug extract effectively reduced both cytokine, IL-6, and TNF-α levels after 7 and 14 days post-wound exposure in comparison with the control group. Similarly, [53] reported that the calophyllolide compound produced from *Calophyllum inophyllum* has the ability to modulate inflammatory cytokine responses by reducing the levels of proinflammatory cytokines such as IL-1β, IL-6, and TNF-α. These suggested a potential anti-inflammatory effect associated with calophylloid. Additionally, [54] found that the mucus produced by the slug mollusk *Arion subfuscus* could lower the expression of some proinflammatory cytokines such as IL-6, TNF-α, and IL-1β. The pleomorphic cytokine IL10 showed anti-inflammatory qualities, and different stimulated immune cells may contribute to its secretion [36]. Its principal functions include anti-inflammatory, inhibitory, or self-regulatory. Interleukin-10 serves as a potent detrimental feedback regulator crucial for the management and resolution of inflammation via autocrine and paracrine mechanisms. IL-10 has two arms that drive a broad immunosuppressive effect, preventing dendritic cells from presenting antigens and preventing the activation of macrophages and their infiltration into the injured area, with the secondary target of reducing the expression of pro-inflammatory cytokines [55]. Additionally, human antigen R (HuR) is a messenger RNA (mRNA) stabilizing protein. It is thought that IL-10 functions as a posttranscriptional regulatory agent at the cellular level to repress HuR and encourage the destabilization of inflammatory cytokine mRNA [56]. The present study showed that slug extract could increase IL-10 levels after 7 and 14 days post-wound exposure in comparison with the control. Comparable findings were noted by [57], who concluded that calophyllolide isolated from *Calophyllum inophyllum* Linn could up-regulate an anti-inflammatory cytokine, IL-10. Collectively, it is evident that slug extract promotes faster wound healing by anti-inflammatory actions, specifically by controlling inflammatory cytokines. The cytokine concentrations are relatively high because the measurements were taken in the wound tissue homogenates instead of serum. Tissue homogenates from an actively infected, inflamed wound site will exhibit a concentrated, localized cytokine milieu, yielding higher absolute values compared to systemic levels [58]. The *in vivo* results of this study painted a clear picture of a sophisticated immunomodulatory effect: The slug extract concurrently suppressed the pro-inflammatory cytokines TNF-α and IL-6 while enhancing the anti-inflammatory cytokine IL-10. The molecular docking investigation provides a compelling, multivalent mechanistic framework that explains how this balanced immune response could be achieved at the molecular level. The findings suggest that the extract does not act as a blunt instrument, but rather as a cocktail of regulatory molecules that differentially interact with key players in the inflammatory cascade. The predicted inhibition of the pro-inflammatory cytokines is primarily driven by the organophosphorus compounds 11 (phenol phosphite) and 12 (TDTBPP), with support from 10 (cholesterol). Compound 11 emerged as the most potent theoretical binder to TNF-α (B.E. −6.663 kcal/mol). Its ability to form a stable π- Stacking interaction with Tyr119 was particularly significant, as this residue was known to be critical for the structural integrity and receptor-binding function of TNF-α [59]. By occupying this site, compound 11 could sterically hinder the trimerization of TNF-α or its binding to the TNFR1 receptor, effectively neutralizing its pro-inflammatory signaling. Similarly, the binding of compound 12

to IL-6 suggested a mechanism for disrupting the IL-6/IL-6R/gp130 signaling complex, which is central to chronic inflammation [60]. The ability of multiple major components of the extract to bind these targets suggests a synergistic blockade of pro-inflammatory pathways. Several limitations should be acknowledged. First, this study utilized a crude chloroform extract containing multiple compounds; batch-to-batch variability in natural product extracts may affect the reproducibility. Standardization of extraction protocols and chemical profiling is needed for future therapeutic development. The use of a crude chloroform extract, rather than purified individual compounds, means that the specific contribution of each constituent to the observed bioactivities cannot be determined. Therefore, the possibility of additive, cooperative, or synergistic interactions among the constituents remains to be experimentally evaluated. Second, while molecular docking provides mechanistic hypotheses, these predictions require experimental validation through direct binding assays (SPR, nuclear magnetic resonance (NMR)) and functional enzymatic inhibition studies. Although several compounds showed favorable predicted binding energies and plausible interactions with DNA gyrase and cytokine targets, these findings cannot establish direct enzyme inhibition, receptor antagonism, or cytokine modulation. Third, the specific contributions of individual compounds (particularly TDTBPP and the phenol phosphite derivative) remain to be confirmed through isolation and testing of purified components. Future studies using purified compounds, biochemical binding assays, enzymatic inhibition assays, and appropriate cellular or functional models are required to validate these computational predictions. Fourth, although the wound measurements were performed by blinded investigators, formal randomization of group allocation and blinding during extract application could be strengthened in future studies. Fifth, the study focused on a single bacterial strain (*S. aureus* ATCC 6538). Therefore, the findings may not be generalizable to other clinically relevant wound pathogens. Further studies are needed to assess the activity of the extract against a broader range of clinical isolates, including methicillin-resistant *S. aureus* (MRSA), as well as polymicrobial biofilms. In addition, comparative studies with clinically established wound-healing and antimicrobial therapies, such as silver sulfadiazine, mupirocin, and hyaluronic acid-based formulations, are warranted to better evaluate the relative therapeutic efficacy and translational potential of the slug extract. A further limitation is that a specific solvent control was not included in the MIC assay. Although chloroform was removed by rotary evaporation before testing, future studies should include an appropriate solvent control to confirm that the observed antibacterial activity is attributable to the slug extract rather than any potential residual solvent effect. Additionally, the observed acceleration of wound closure was accompanied by a reduction in the bacterial burden in the treated wounds after 7 days; however, the persistence of this antibacterial effect beyond day 7 remains unknown. Reduced bacterial colonization may indirectly contribute to a more favorable environment for tissue repair by limiting persistent infection and inflammation. Nevertheless, the present experimental design does not allow us to determine whether the improved wound closure directly resulted from regenerative effects of the extract, indirectly from its antibacterial activity, or from a combination of these effects. Further studies using experimental designs that separately evaluate antibacterial and tissue-regenerative activities are required to clarify this relationship.

Finally, while extensive *in vitro* cytotoxicity profiling (e.g., MTT assays) and systemic multi-organ biochemical evaluations were beyond the immediate scope of this primary efficacy study, preliminary safety profiles were monitored in a macroscopic manner. No clinical signs of systemic toxicity, abnormal behavioral changes, or treatment related mortality were observed in the experimental animals during the 14 days' experimental period following topical application of the *Laevicaulis alte* extract. In addition, the local tissue tolerance was excellent. A histological analysis of the wound bed demonstrated a normal inflammatory resolution phase with no evidence of severe local

necrosis, foreign body reactions, or excessive tissue damage. However, immediate objectives of the next phase of our research are comprehensive histopathological screening of multiple organs (e.g., liver and kidney H&E staining) and standard cellular cytotoxicity assays to fully establish the systemic biosafety margin of this bioactive extract prior to clinical applications.

5. Conclusions

In conclusion, the present study demonstrated that the chloroform extract of *Laevicaulis alte* exhibited antibacterial activity against *Staphylococcus aureus* and was associated with accelerated wound closure, reduced bacterial burden, modulation of inflammatory cytokines, and changes in collagen deposition in an infected murine wound model. A GC–MS analysis identified several chemical constituents, with TDTBPP and cholesterol representing the most abundant detected compounds. Additionally, molecular docking predicted that several identified constituents could favorably interact with bacterial DNA gyrase and selected cytokine targets. However, these computational findings should be considered hypothesis-generating and cannot establish direct target inhibition or the individual contribution of specific compounds to the observed biological effects. Similarly, the present study does not establish whether the improvement in wound healing resulted directly from tissue-regenerative activity, indirectly from reduced bacterial burden, or from a combination of effects. Further studies using purified compounds, biochemical and functional assays, and standardized extract preparations are needed to validate the mechanisms and therapeutic potential of *L. alte* extract and determine which compounds were responsible for the extract efficacy.

Use of AI tools declaration

We declare that we have not used Artificial Intelligence (AI) tools in the creation of this article.

Ethics approval and consent to participate

Care and ethical use of experimental animals, which were approved by Helwan university's Animal Ethics Committee and assigned the study ethics number [HU-IACUC/Z/MY3107-31]. This study was done in accordance with ARRIVE guidelines (https://arriveguidelines.org).

Consent for publication

This study didn't include any human participants, and all methods were done on mice.

Availability of data and materials

The datasets used and/or analyzed during the current study are available from the corresponding author on reasonable request.

Conflict of interest

The authors declare that there are no competing interests associated with the manuscript.

Acknowledgements

We would like to than Princess Nourah bint Abdulrahman University, Riyadh, Saudi Arabia, for supporting tis research. This research was funded by Princess Nourah bint Abdulrahman University Researchers Supporting Project number (PNURSP2026R83), Princess Nourah bint Abdulrahman University, Riyadh, Saudi Arabia.

Author contributions

Mostafa Morad: Conceptualization, Methodology, Writing—original draft, Investigation, Data curation, Formal analysis, Writing—review & editing. Heba Elsayed: Conceptualization, Methodology, Writing—original draft, Investigation, Data curation, Formal analysis, Writing—review & editing. Ahmed El Hennawy: Conceptualization, Methodology, Writing—original draft, Investigation, Data curation, Formal analysis, Writing—review & editing. Hana Sonbol: Resources, Project administration, Writing—original draft. Olfat Hammam: Conceptualization, Methodology, Writing—original draft, Investigation, Data curation, Formal analysis, Writing—review & editing. Asmaa Abdelmonem: Conceptualization, Methodology, Writing—original draft, Investigation, Data curation, Formal analysis, Writing—review & editing. Amina Ibrahim: Conceptualization, Methodology, Writing—original draft, Investigation, Data curation, Formal analysis, writing—review & editing. Marwa A. Hamada: Conceptualization, Methodology, Writing—original draft, Investigation, Data curation, Formal analysis, Writing—review & editing. All authors have read and agreed to the published version of the manuscript.

References

1. Sounouvou HT, Toukourou H, Catteau L, et al. (2021) Antimicrobial potentials of essential oils extracted from West African aromatic plants on common skin infections. *Sci Afr* 11: e00706. https://doi.org/10.1016/j.sciaf.2021.e00706
2. Abdo JM, Sopko NA, Milner SM (2020) The applied anatomy of human skin: A model for regeneration. *Wound Med* 28: 100179. https://doi.org/10.1016/j.wndm.2020.100179
3. Canchy L, Kerob D, Demessant AL, et al. (2023) Wound healing and microbiome, an unexpected relationship. *J Eur Acad Dermatology Venereol* 37: 7–15. https://doi.org/10.1111/jdv.18854
4. Agyei MK, Sakyi SA, Annan JJ, et al. (2024) Dermatologic diseases in Africa: The profile of patients attending a tertiary hospital in the Ashanti Region of Ghana. https://doi.org/10.21203/rs.3.rs-5296285/v1
5. Wilkinson HN, Hardman MJ (2020) Wound healing: Cellular mechanisms and pathological outcomes. *Open Biol* 10: 200223. https://doi.org/10.1098/rsob.200223
6. Raziyeva K, Kim Y, Zharkinbekov Z, et al. (2021) Immunology of acute and chronic wound healing. *Biomolecules* 11: 700. https://doi.org/10.3390/biom11050700
7. Gupta NK, Paul P, Barman H, et al. (2023) The marsh slug, Deroceras laeve in Darjeeling Himalayas, India: First record and modelling of suitable habitats. *Acta Ecol Sin* 43: 432–438. https://doi.org/10.1016/j.chnaes.2022.07.003
8. Kumar P (2020) A review—on molluscs as an agricultural pest and their control. *Int J Food Sci Agric* 4: 383–389. http://doi.org/10.26855/ijfsa.2020.12.004

9. Bruelheide H, Scheidel U (1999) Slug herbivory as a limiting factor for the geographical range of Arnica montana. *J Ecol* 87: 839–848. https://doi.org/10.1046/j.1365-2745.1999.00403.x
10. Hanley ME (1998) Seedling herbivory, community composition and plant life history traits. *Perspect Plant Ecol Evol Syst* 1: 191–205. https://doi.org/10.1078/1433-8319-00058
11. Pawlik JR (2011) The chemical ecology of sponges on Caribbean reefs: Natural products shape natural systems. *Bioscience* 61: 888–898. https://doi.org/10.1525/bio.2011.61.11.8
12. Al Naggar Y, Fahmy NM, Alkhaibari AM, et al. (2025) Mechanisms and genetic drivers of resistance of insect pests to insecticides and approaches to its control. *Toxics* 13: 681. https://doi.org/10.3390/toxics13080681
13. Rashad M, Sampò S, Cataldi A, et al. (2023) Biological activities of gastropods secretions: Snail and slug slime. *Nat Prod Bioprospect* 13: 42. https://doi.org/10.1007/s13659-023-00404-0
14. Rashad M, Sampò S, Cataldi A, et al. (2025) From nature to nurture: The science and applications of snail slime in health and beauty. *J Cosmet Dermatol* 24: e70002. https://doi.org/10.1111/jocd.70002
15. Ibrahim AM, Hamed AA, Ghareeb MA (2021) Marine, freshwater, and terrestrial snails as models in the biomedical applications. *Egypt J Aquat Biol Fish* 25: 23–38. https://doi.org/10.21608/ejabf.2021.172142
16. Clinical and Laboratory Standards Institute (CLSI) (2021) M100: Performance standards for antimicrobial susceptibility testing.
17. Balouiri M, Sadiki M, Ibnsouda SK (2016) Methods for *in vitro* evaluating antimicrobial activity: A review. *J Pharm Anal* 6: 71–79. https://doi.org/10.1016/j.jpha.2015.11.005
18. Alfei S, Torazza C, Bacchetti F, et al. (2025) Tri-Phenyl-Phosphonium-Based nano vesicles: A new *in vitro* nanomolar-active weapon to eradicate PLX-Resistant melanoma cells. *Int J Mol Sci* 26: 3227. https://doi.org/10.3390/ijms26073227
19. El-Sayed H, Morad MY, Sonbol H, et al. (2023) Myco-synthesized selenium nanoparticles as wound healing and antibacterial agent: An *in vitro* and *in vivo* investigation. *Microorganisms* 11: 2341. https://doi.org/10.3390/microorganisms11092341
20. Rhea L, Dunnwald M (2020) Murine excisional wound healing model and histological morphometric wound analysis. *J Vis Exp* 162: e61616. https://doi.org/10.3791/61616
21. Sato H, Ebisawa K, Takanari K, et al. (2015) Skin-derived precursor cells promote wound healing in diabetic mice. *Ann Plast Surg* 74: 114–120. https://doi.org/10.1097/SAP.0000000000000342
22. Khalaf AA, Hassanen EI, Zaki AR, et al. (2019) Histopathological, immunohistochemical, and molecular studies for determination of wound age and vitality in rats. *Int Wound J* 16: 1416–1425. https://doi.org/10.1111/iwj.13206
23. Chang JYF, Kessler HP (2008) Masson trichrome stain helps differentiate myofibroma from smooth muscle lesions in the head and neck region. *J Formos Med Assoc* 107: 767–773. https://doi.org/10.1016/S0929-6646(08)60189-8
24. Chen Y, Yu Q, Xu CB (2017) A convenient method for quantifying collagen fibers in atherosclerotic lesions by ImageJ software. *Int J Clin Exp Med* 10: 14927–14935.
25. Landini G, Martinelli G, Piccinini F (2021) Colour deconvolution: Stain unmixing in histological imaging. *Bioinformatics* 37: 1485–1487. https://doi.org/10.1093/bioinformatics/btaa847
26. Saeed S, Martins-Green M (2024) Assessing animal models to study impaired and chronic wounds. *Int J Mol Sci* 25: 3837. https://doi.org/10.3390/ijms25073837

27. Khalil RG, Ibrahim AM, Bakery HH (2022) Juglone: A novel immunomodulatory, antifibrotic, and schistosomicidal agent to ameliorate liver damage in murine schistosomiasis mansoni. *Int Immunopharmacol* 113: 109415. https://doi.org/10.1016/j.intimp.2022.109415
28. National Center for Biotechnology Information (2026) PubChem compound summary for CID 41209: 2,6,10,15-Tetramethylheptadecane. PubChem. Available from: https://pubchem.ncbi.nlm.nih.gov/compound/2_6_10_15-Tetramethylheptadecane. Accessed 5 October 2026.
29. Taskin H (2013) Detection of volatile aroma compounds of Morchella by headspace gas chromatography mass spectrometry (HS-GC/MS). *Not Bot Horti Agrobot Cluj-Napoca* 41: 122–125. https://doi.org/10.15835/nbha4118344
30. Siswadi S, Saragih GS (2021) Phytochemical analysis of bioactive compounds in ethanolic extract of Sterculia quadrifida R. Br. *AIP Conf Proc* 2353: 030098. https://doi.org/10.1063/5.0053057
31. Belakhdar G, Benjouad A, Abdennebi EH, et al. (2015) Determination of some bioactive chemical constituents from Thesium humile Vahl. *J Mater Environ Sci* 6: 2778–2783.
32. Zhang K, Li T, Shan X, et al. (2021) Cholesterol: Bioactivities, structural modification, mechanisms of action, and structure-activity relationships. *Mini Rev Med Chem* 21: 1830–1848. https://doi.org/10.2174/1389557521666210105123320
33. Taher MA, Laboni AA, Shompa SA, et al. (2023) Bioactive compounds extracted from leaves of G. cyanocarpa using various solvents in chromatographic separation showed anti-cancer and anti-microbial potentiality in *in silico* approach. *Chinese J Anal Chem* 51: 100336. https://doi.org/10.1016/j.cjac.2023.100336
34. Vinuchakkaravarthy T, Kumaravel KP, Ravichandran S, et al. (2011) Active compound from the leaves of Vitex negundo L. shows anti-inflammatory activity with evidence of inhibition for secretory phospholipase A2 through molecular docking. *Bioinformation* 7: 199. https://doi.org/10.6026/97320630007199
35. Zhao Y, Wang Q, Yan S, et al. (2021) Bletilla striata polysaccharide promotes diabetic wound healing through inhibition of the NLRP3 inflammasome. *Front Pharmacol* 12: 659215. https://doi.org/10.3389/fphar.2021.659215
36. Saraiva M, O'Garra A (2010) The regulation of IL-10 production by immune cells. *Nat Rev Immunol* 10: 170–181. https://doi.org/10.1038/nri2711
37. Ibrahim AM, Morad MY, El-Khadragy MF, et al. (2022) The antioxidant and anti-inflammatory effects of Eremina desertorum snail mucin on experimentally-induced intestinal inflammation and testicular damage. *Biosci Rep* 42: BSR20221020. https://doi.org/10.1042/BSR20221020
38. Ulagesan S, Kim HJ (2018) Antibacterial and antifungal activities of proteins extracted from seven different snails. *Appl Sci* 8: 1362. https://doi.org/10.3390/app8081362
39. Bax BD, Chan PF, Eggleston DS, et al. (2010) Type IIA topoisomerase inhibition by a new class of antibacterial agents. *Nature* 466: 935–940. https://doi.org/10.1038/nature09197
40. Liu C, Xu Y, Lu Y, et al. (2022) Mesenchymal stromal cells pretreated with proinflammatory cytokines enhance skin wound healing via IL-6-dependent M2 polarization. *Stem Cell Res Ther* 13: 414. https://doi.org/10.1186/s13287-022-02934-9
41. Aldred KJ, Kerns RJ, Osherof N (2014) Mechanism of quinolone action and resistance. *Biochemistry* 53: 1565–1574. https://doi.org/10.1021/bi5000564
42. Pietrusiński M, Stączek P (2006) Bacterial type II topoisomerases as targets for antibacterial drugs. *Postepy Biochem* 52: 271–282.

43. He MM, Smith AS, Oslob JD, et al. (2005) Small-molecule inhibition of TNF-α. *Science* 310: 1022–1025. https://doi.org/10.1126/science.1116304
44. Somers W, Stahl M, Seehra JS (1997) 1.9 Å crystal structure of interleukin 6: Implications for a novel mode of receptor dimerization and signaling. *EMBO J* 16: 989–997. https://doi.org/10.1093/emboj/16.5.989
45. Yoon SI, Jones BC, Logsdon NJ, et al. (2005) Same structure, different function: Crystal structure of the Epstein-Barr virus IL-10 bound to the soluble IL-10r1 chain. *Structure* 13: 551–564. https://doi.org/10.1016/j.str.2005.01.016
46. Chinemerem Nwobodo D, Ugwu MC, Oliseloke Anie C, et al. (2022) Antibiotic resistance: The challenges and some emerging strategies for tackling a global menace. *J Clin Lab Anal* 36: e24655. https://doi.org/10.1002/jcla.24655
47. Guedes BN, Krambeck K, Durazzo A, et al. (2024) Natural antibiotics against antimicrobial resistance: Sources and bioinspired delivery systems. *Braz J Microbiol* 55: 2753–2766. https://doi.org/10.1007/s42770-024-01410-1
48. Aditya G, Paul P (2022) Observations on the growth and life table estimates of the slug Mariaella dussumieri (L. Pfeiffer, 1855) (Gastropoda: Ariophantidae). *Zool Ecol* 32: 136–143. https://doi.org/10.35513/21658005.2022.2.6
49. Sallam AAA, El-Massry SA, Nasr IN (2009) Chemical analysis of mucus from certain land snails under Egyptian conditions. *Arch Phytopathol Plant Prot* 42: 874–881. https://doi.org/10.1080/03235400701494448
50. Lanz MA, Klostermeier D (2012) The GyrA-box determines the geometry of DNA bound to gyrase and couples DNA binding to the nucleotide cycle. *Nucleic Acids Res* 40: 10893–10903. https://doi.org/10.1093/nar/gks852
51. Wagner H (2011) Synergy research: Approaching a new generation of phytopharmaceuticals. *Fitoterapia* 82: 34–37. https://doi.org/10.1016/j.fitote.2010.11.016
52. Errajouani F, Bakrim H, Hourfane S, et al. (2023) Exploring the potential anti-inflammatory and wound-healing proprieties of *Cepaea hortensis* Snail Mucin. *Cosmetics* 10: 170. https://doi.org/10.3390/cosmetics10060170
53. Ferdosh S (2024) The extraction of bioactive agents from Calophyllum inophyllum L., and their pharmacological properties. *Sci Pharm* 92: 6. https://doi.org/10.3390/scipharm92010006
54. Deng T, Gao D, Song X, et al. (2023) A natural biological adhesive from snail mucus for wound repair. *Nat Commun* 14: 396. https://doi.org/10.1038/s41467-023-35907-4
55. Porro C, Cianciulli A, Panaro MA (2020) The regulatory role of IL-10 in neurodegenerative diseases. *Biomolecules*10: 1017. https://doi.org/10.3390/biom10071017
56. Wills-Karp M, Nathan A, Page K, et al. (2010) New insights into innate immune mechanisms underlying allergenicity. *Mucosal Immunol* 3: 104–110. https://doi.org/10.1038/mi.2009.138
57. Nguyen VL, Truong CT, Nguyen BCQ, et al. (2017) Anti-inflammatory and wound healing activities of calophyllolide isolated from *Calophyllum inophyllum* Linn. *PLoS One* 12: e0185674. https://doi.org/10.1371/journal.pone.0185674
58. Verlinden W, Francque S, Vonghia L (2017) Peripheral venous, portal venous, hepatic venous, and arterial and intrahepatic cytokine levels as biomarkers and functional correlations, In: *Biomarkers in Liver Disease*, Dordrecht: Springer, 581–602. https://doi.org/10.1007/978-94-007-7675-3_22

59. Van Ostade X, Tavernier J, Prangé T, et al. (1991) Localization of the active site of human tumour necrosis factor (hTNF) by mutational analysis. *EMBO J* 10: 827–836. https://doi.org/10.1002/j.1460-2075.1991.tb08015.x
60. Hunter CA, Jones SA (2015) IL-6 as a keystone cytokine in health and disease. *Nat Immunol* 16: 448–457. https://doi.org/10.1038/ni.3153



AIMS Press

© 2026 the Author(s), licensee AIMS Press. This is an open access article distributed under the terms of the Creative Commons Attribution License (https://creativecommons.org/licenses/by/4.0)